DOKUZ EYLÜL UNIVERSITY
GRADUATE SCHOOL OF NATURAL AND APPLIED SCIENCES

INVESTIGATION OF THE EFFECT OF CARBON AND TITANIA ADDITIONS ON THE MECHANICAL THERMAL AND MICROSTRUCTURAL PROPERTIES OF HIGH ALUMINA REFRACTORIES

by
Irmak Su ÖKTEN

January, 2021
İZMİR

INVESTIGATION OF THE EFFECT OF CARBON AND TITANIA ADDITIONS ON THE MECHANICAL THERMAL AND MICROSTRUCTURAL PROPERTIES OF HIGH ALUMINA REFRACTORIES

A Thesis Submitted to the
Graduate School of Natural and Applied Sciences of Dokuz Eylül University
In Partial of the Requirements for the Degree of Master of
Science in Metallurgical and Materials Program

by
Irmak Su ÖKTEN

January, 2021
İZMİR

M.Sc THESIS EXAMINATION RESULT FORM

We have read the thesis entitled **"INVESTIGATION OF THE EFFECT OF CARBON AND TITANIA ADDITIONS ON THE MECHANICAL THERMAL AND MICROSTRUCTURAL PROPERTIES OF HIGH ALUMINA REFRACTORIES"** completed by **IRMAK SU ÖKTEN** under supervision of **PROF.DR. ALİ AYDIN GÖKTAŞ** and we certify that in our opinion it is fully adequate, in scope and in quality, as a thesis for the degree of Master of Science.

Prof. Dr. Ali Aydın GÖKTAŞ

Supervisor

Asst. Prof. Dr. Bahadır UYULGAN

(Jury Member)

Assoc. Prof. Dr. Mücahit SÜTÇÜ

(Jury Member)

Prof. Dr. Özgür ÖZÇELİK

Director

Graduate School of Natural and Applied Sciences

ACKNOWLEDGEMENT

My very special thanks to Prof. Dr. Ali Aydın Göktaş for his constant help throughout the thesis, instucting technical issues and his guidance in all areas.

I express my sincere thanks to my dear friend Dt. Buse Demir who passed away due to Aegean Sea earthquake and her dear mother Şaziye Demir for being always loving, kindly, motivator and inspiring to me.

I would like to thank my family members Haluk Ökten, Nurşen Ökten, Pınar Eylül Ökten, Derya Güz Ökten and Erdem Acar for their supports, sensibilities and affection.

Irmak Su ÖKTEN

INVESTIGATION OF THE EFFECT OF CARBON AND TITANIA ADDITIONS ON THE MECHANICAL THERMAL AND MICROSTRUCTURAL PROPERTIES OF HIGH ALUMINA REFRACTORIES

ABSTRACT

High alumina refractories are used in industrial type aluminium melting furnaces operated with molten aluminium alloys. One of the biggest failures of high alumina refractory materials during melting is corundum (alumina) formation. This defect in refractories leads to reduction in efficiency of melting process by furnace's volume decrease, thereby increasing in cost. In this study, different types of additives were added to high alumina refractory samples in order to improve the performance of refractory material. To restrain this defect, containing graphite and titania additive refractory bricks were produced. Obtained refractory bricks are investigated by means of mechanical, physical, thermal and chemical properties with the test methods of cold and hot crushing strength, bulk density, apparent porosity, thermal shock and corrosion test. Microstructure and phase development of the samples were analyzed by scanning electron microscope (SEM), X-ray diffraction (XRD) analyses, respectively.

Keywords: Refractories, titania, carbon, corrosion, aluminium melting furnace

TİTANYA VE KARBON KATKISININ YÜKSEK ALÜMİNALI TUĞLALARININ MEKANİK TERMAL VE MİKROYAPISAL ÖZELLİKLERİNE ETKİSİNİN İNCELENMESİ

ÖZ

Endüstriyel alüminyum ergitme fırınları duvarlarında yüksek alüminalı refrakterler kullanılır. Ergitme sırasında yüksek alüminalı refrakter malzemede karşılaşılan en büyük sorunlardan biri korund (alümina) oluşumudur. Refrakterdeki bu kusur, fırın hacmini azaltarak ergitme sürecinin verimliliğini düşürür ve maliyet artışına sebep olur. Bu çalışmada, refrakter malzemenin performansını iyileştirmek amacıyla farklı tip katkılar yüksek alüminalı refrakter tozuna eklenmiştir. Korund problemini önlemek için grafit ve titanya tozları kullanılmıştır. Bu tozlar karakterize etmek ve değerlendirmek üzere tuğla numuneler haline getirilmişlerdir. Elde edilen refrakter tuğlalar, mekanik, fiziksel, termal ve kimyasal olarak, sırasıyla, soğuk ve sıcak kırılma mukavemeti, hacim yoğunluk, görünür porozite, termal şok ve korozyon test metotlarıyla incelenmişlerdir. Numunelerin mikroyapı ve faz gelişimleri sırasıyla taramalı elektron mikroskobu ve X-ışını kırınımı metotlarıyla analiz edilmiştir.

Anahtar kelimeler: Rekrakterler, titanya, karbon, korozyon, alüminyum ergitme fırını

CONTENTS

Page

LIST OF FIGURES

Page

LIST OF TABLES

Page

CHAPTER 1
INTRODUCTION

1.1 Background

The problem of molten aluminum incorporated into alumina-silicate refractories was first noted with the traditional pot test by Brondyke (1953)**.** Studies in alumina silicate refractories exposured to molten aluminium exhibited aluminum wetting property. Research results show that melting penetration of aluminum in form of edge wall formations occurs as a result of reactions of compounds containing aluminum with silica in alumina-silicate refractories.

A stress occurs at the metal level due to an increase in volume caused from the formation of aluminium oxide (corundum) as penetration product. The presence of this tensile stress induces cracks in the refractory. It was understood that the original alumina aggregates were damaged by aluminum metal penetration and its interaction with silica in the refractory matrix in the studies of Hemrick et al. (2008).

In the study by Allaire (2000), the existence of the two spesific condition in bellyband area is stated: First condition is the existence of a triple system consisting of metal/solid/refractory and gas atmosphere. The second condition is the thermal gradient. In the study, it is stated that temperatur below the metal level is 800 ^{o}C and this reaches 1300 °C on the side walls above the metal level. In aluminum melting furnaces, bellyband zone, metal level or below metal level creates corrosion in molten aluminum refractory, while corundum formation above metal level causes damage to the material and reduces the furnace volume. These formations reduce the efficiency of the process and increase costs (Allaire, 2000).

There are some additives used to improve properties of alumina refractories. The addition of titanium oxide produced a relatively uniform, dense microstructure at high temperature. Chen et al. (2012) stated alumina is one of the major constituent in this class of refractories, which is necessary to provide mechanical and thermomechanical properties. De Villiers et al. (2020) expressed that tetravalent cation oxides such as TiO_2 greatly improve the spinel sintering process as they decrease the synthesis

temperature, and also increase the thermodynamic stability of the spinel solid solution phase. Furthermore, it is stated that the addition of appropriate amounts of TiO_2, generally up to 2%, can significantly increase the spinel densification (Yuan et al., 2017).

An another additive utilized in melting and holding furnaces is the graphite. Graphite is used as a primary carbon source, which provides high corrosion resistance by avoiding adhesion of steel, and slag melts because of its nonwetting nature furthermore it improves thermal shock resistance because of its high thermal conductivity and low thermal expansion. As for Wei et al. (2020) report that the solid reaction between Al_2O_3 and carbon will not occur below 2220 °C at atmospheric pressure in the air. Thus, the reaction of solid Al_2O_3 and carbon was ignored in aluminium melting process which was usually proceeded at a much lower temperature. In the study by Juhasz et al. (2013), it is expressed that liquid aluminium does not wet graphite even under an existence of molten salt which is able to remove the oxide layer from the Al/C interface. In this thesis**,** graphite was added into refratory mixture starting from these studies' point of view.

In aluminum production, the durability of the refractory material is great importance. The resistance of refractory to aluminum penetration is vital, specially when it comes to contact with melting aluminum as alloy.

In this study, it is aimed to improve the resistancy of used refractories against to the aluminium penetration. To achieve these goals alumina silicate refractories were produced with the additives of titania and graphite. The samples prepared in this study were subjected to corrosion and refractoriness tests and the necessary microstructural and thermal analyzes and evaluations were made regarding the results.

CHAPTER 2
DESCRIPTION AND CLASSIFICATION OF REFRACTORY MATERIALS

2.1 Refractory Materials

Refratory materials do not lose their physical and chemical properties against mechanical impact and friction effects, and have durability to high temperatures. Refractory materials are resistant to all kinds of corrosive materials like molten metal, slag, acid, etc.

Refractories are widely used in the industry in all processes where high temperatures are required for the purpose of protecting and isolating the construction due to these properties. There is no other type of material thats working conditions can be so variable.

There are six essential oxides that can be used as refractory materials. These are SiO_2 (Silica), Al_2O_3 (Alumina), MgO (Magnesia), CaO (Calcia), Cr_2O_3 (Chromia) and ZrO_2 (Zirconia). The number of variety increases with the materials of different composition that they form with each other.

Refractory materials can be classified in general as acidic, neutral or basic according to their chemical composition (Yılmaz et al., 2016).

2.2 Classification Of Refractories

Refractory materials are classifed according to their chemical and physical propert ies, producing methods and physical conditions, in various ways. Temperature, type of refractory material, chemical properties, resources of raw materials, production process, physical structure, etc. classifications made on the basis of the issues that are present (Yılmaz et al., 2016).

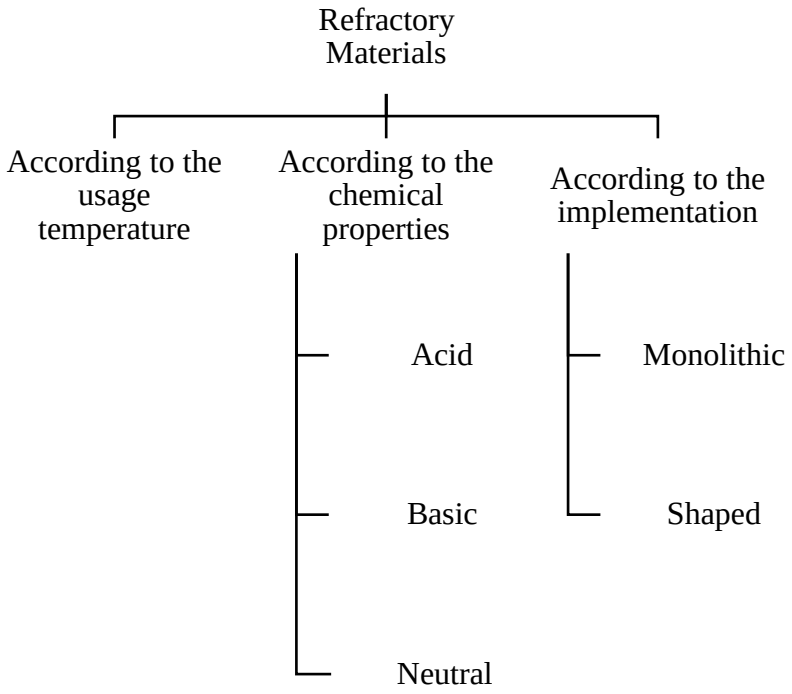

Figure 2.1 Classification of refractory materials

2.2.1 Classification Based On Usage Temperature

Classification of refractories acccording to usage temperature is given below:

a) Standard service refractories (1580 – 1780 °C)

b) Heavy service refractories (1780 – 2000 ° C)

c) Super service refractories (> 2000 ° C)

2.2.2 Classification Based On Implementation

Refractory materials are evaluated as shaped refractory materials and monolithic refractory materials according to the production methods.

2.2.2.1 Shaped Refractories

This refractory group is composed of brick and plate refractories. Generally, they are produced by press or extrution method.

2.2.2.2 Monolithic Refractories

The amorphous substance obtained by combining various refractory raw material granules (chamotte, bauxite, mullite, alumina, magnesite, etc.) with suitable binders is called monolithic material in the correct combining ratios of grain size. Monolithic materials are being more and more common in recent years. Among the reasons for this, the importance of monolithic materials such as ease of application and repair, low labor usage, low costs, short stoppages at the application site, and the performance of the developed materials close to shaped products have played an important role.

2.2.3 Classification Based On Chemical Properties

The following is description of refractory materials according to their chemical properties.

2.2.3.1 Acid Refractories

The refractories used in this group include primarily group RO_2. (Group R shows only five valence elements or three valence elements. Accordingly, according to their materials, acid refractory bricks are called as follows. Acidic refractories are also called "Alumina Silicates" due to this classification.

- Chamotte (SiO_2. Al_2O_3)
- Silica (SiO_2)
- Sillimanite (Al_2O_3. SiO_2)
- Mullite ($3Al_2O_3$. $2SiO_2$)
- Zircon (ZrO_2. SiO_2)

2.2.3.2 Basic Refractories

Refractory bricks falling into this group comprise mostly group RO. Specific refra ctory bricks are often called as follows according to their material.

- Chrome (MgO. Cr_2O_3. Al_2O_3. FeO)
- Magnesia (MgO)
- Dolomite (MgO. CaO)

- Magnesia chrome
- Chrome magnesia

2.2.3.3 Neutral Refractories

Refractory bricks that fall into this group mainly contain the R_2O_3 or RO. R_2O_3 group. Neutral refractory bricks are named according to their contents as follows. Information on high alumina refractories are presented in Chapter 5.

- Bauxite ($Al_2O_3H_2O$ or $Al_2O_3.3H_2O$)
- Alumina (AI_2O_3)
- Carbon (pitch, graphite, tar)
- Chromite (Cr_2O_3)
- Spinel (Al_2O_3. MgO)
- Pichrochromite (MgO. Cr_2O_3)

General information about refractory materials is provided in chapter two.

CHAPTER 3
ALUMINIUM MELTING PROCESS

3.1 Introduction

The beginning of aluminum production is the method by which Bayer transforms bauxite into alumina. After that alumina is melted with the addition of cryolite or Al-fluorite and then electrolysis to aluminium. Raw (untreated) aluminum ingots have become popular in recent years, and many aluminum products are produced by remelting of raw aluminium in its melting and holding furnaces. There are many aluminum smelting and holding processes in the literature. Commercial purity (higher than 99% purity) aluminum has a melting point of around 650- 660 °C. Generally, the temperture which is used in melting furnaces is 730°C (Furness & Pygall, 1983).

3.2 Aluminium Melting Furnaces And Refractories

3.2.1 Aluminium Melting Furnace

There are different types of furnaces used to melt aluminium. These can be seen in Table 3.1 (Car, 2008). Two different kinds of operation are done in the foundry work, the regular melting operation and the combined holding operation. Different types of furnaces can be found according to the conditions and purification applications.

Table 3.1 Conformity of furnace selection to aluminum plants (Car, 2008)

Combustion based furnaces	**Secondary plants**		**Partial secondary plants**		**Foundries**		**Primary plants**	
	Melting	**Holding**	**Melting**	**Holding**	**Melting**	**Holding**	**Melting**	**Holding**
Fixed reverber furnace	3	4	3	4	4	4	0	4
Overhead-fed furnace	3	0	3	0	0	0	0	0
Circular section furnace	0	0	1	1	0	1	0	0
Twin cabin furnace	3	1	3	1	2	1	0	0
Sweating furnace	3	0	1	0	0	0	0	0
Floor heating sweating furnace	3	0	1	0	0	0	0	0
Shaft type furnace	0	0	0	0	3	3	0	0
Tilting reverber furnace	3	4	3	4	4	4	0	4
Barrel type furnace	2	0	2	0	0	0	0	0
Oval furnace	2	0	2	0	0	0	0	0
Pot furnace	0	0	0	0	3	3	0	0
Rotary furnace	4	0	2	0	0	0	0	0
Electrically heated furnaces	**Melting**	**Holding**	**Melting**	**Holding**	**Melting**	**Holding**	**Melting**	**Holding**
Electrically reverber furnace	0	1	0	1	0	1	0	2
Electrically pot furnace	0	0	0	0	3	0	0	0
Channel induction furnace	2	0	2	0	2	0	2	0
Coreless induction furnace	1	2	1	2	1	2	0	1
0: non-utilisable; 1: used special production; 2: used frequently; 3: standard technology; 4: core technology.								

The heat required for heating or melting are obtained by burning fossil fuels ovens. Fuels used in aluminum production processes are natural gas and fuel oil for combustion based furnaces.

As in gas-fired furnaces, there is less chance of slag formation and absorption of hydrogen gas from the molten metal, because there is no burner unit for electrically heated furnaces. It is therefore suitable for higher application of insulation and hence higher energy efficiency. The use of flux, however, must be limited as it will reduce resilience of resistance. Electrically heated furnaces commonly find use in primary facilities as holding furnaces.

3.2.2 Shaft Type Aluminium Melting Furnace

3.2.2.1 Melting Part

In aluminium foundries, especially in die casting foundries shaft melting furnaces are used, for high requirement of metal quality, melting performance and rentability. Figure 3.1 illustrates the constructive structure of a fuel-heated shaft melting furnace for melting and holding aluminium alloys (Gaertner et al., 2015). Thanks to a special shaft geometry and especially to adapted burner technology, the process steps such as preheating, heating and liquefaction can be combined in one melting shaft.

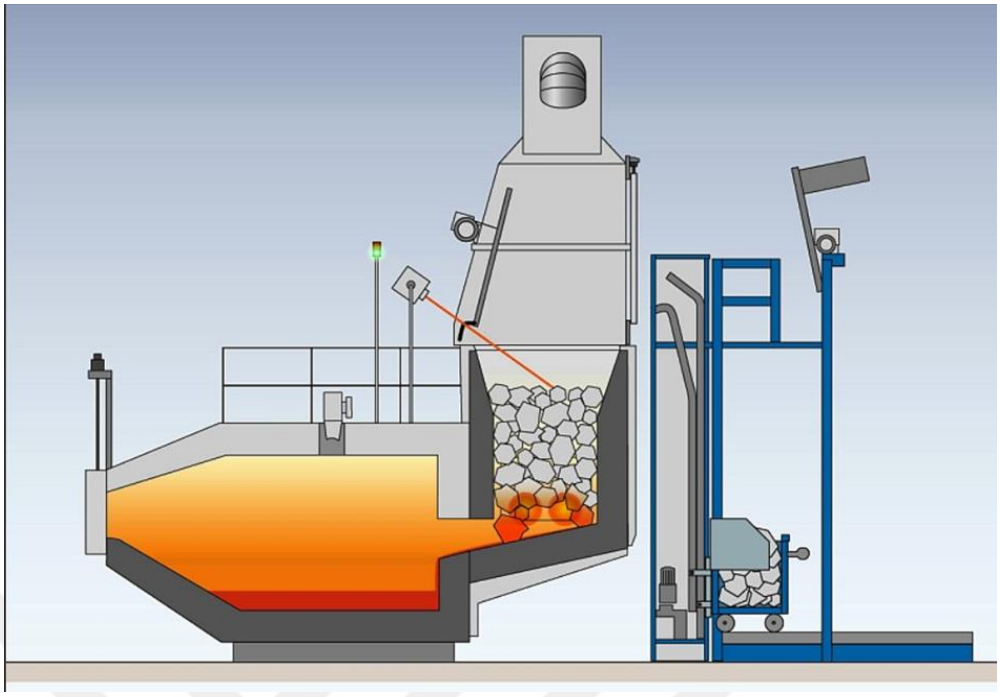

Figure 3.1 Melting Part Schematic structure of a shaft melting furnace (Gaertner et al., 2015)

3.2.2.2 Holding Part

The furnace arrangement with separate burner devices for the melting shaft and/ or holding portion guarantees a continuous metal discharge with a temperature tolerance of ± 5 ° C and allows for versatile metal supply as an essential requirement for good performance for the foundry.

CHAPTER 4
THE ALUMINIUM PENETRATION AND THE CORROSION OF REFRACTORY BY MOLTEN ALUMINIUM

4.1 Introduction

Refractories used metal industries are mostly basic. Key characteristics requirements for these refractories is the resistance to molten slag (basic) and to the high temperature produced during the process. In aluminum industry, the refractory property requirements are quite different from that of steel making. Although the temperature of aluminum refining and alloying process is much lower than for steel, it has the unique problem of penetration in the refractories. Hence, the refractory should be designed in such a way so that it possess a nonwetting characteristic to molten aluminum.

4.2 Wear Mechanisms Of Refractory Materials

Refractory materials are used at high temperatures for a duration of long time and therefore They are exposed to corrosive environments at that high temperatures. They are in contact with molten metal and destructive elements such as slag and abrasive particles. Wear mechanisms in refractories are as follows:

- Abrasion
- Penetration
- Corrosion/ Erosion
- Spalling

Physical, chemical and mechanical factors play an important role in wear mechanisms.

4.2.1 Abrasion

Mechanical wear is known as abrasion of the refractory surface. Mechanism vibration, up and down effects, attacks of particulate or free gasses, occurs during furnace charging, or by the effect of furnace gas wastes. Abrasion is often seen in the loading zones of aluminum furnaces (Banarjee, 1998).

4.2.2 Penetration

Penetration is defined as by moving of gas, liquid or solids from refractory surface into inner particles and it is a corrosive situation. New compounds or phases can form during penetration. Refractory loss occurs with penetration. In aluminum industry the most arising problems is the penetration. Aluminium melt penetrates the refractory matrix which produces corundum. It serves as a backbone for its development. Strong lumps (swells) of corundum crystals form and they reduce furnace volume (Banarjee, 1998).

4.2.3 Corrosion

Corrosion of refractories begin with dissolving in a liquid or vapor; or it may be happen with reactions in a solid form. Corrosion starts with the entry of liquid or vapor into the pores, creating a changed layer (Banarjee, 1998). Corrosion in the refractory involves physical/ mechanical degradation as well as chemical reactions, this is a dynamic occurrence. The decomposition of refractories interacted with metal penetration into the refractory, in ther words dissolution of the refractor in the melt caused by contact with the melt metal. Figure 4.1 shows corrosion on edge walls thereby corundum formation.

In the active part of the corrosion process, reaction products are dissolved in molten metal. In the passive part, a thick continuous solid reaction product layer is formed that reduces the overall speed of corrosion. Corrosion is usually a mixture of those two parts (S. Zhang et al., 2001). The rate of corrosion, diffusion of dissolved refractory material and the formation of phases at the interface are regulated (Meyer-Rau & Telle, 2005).

Figure 4.1 Example of corrosion on edge walls in aluminium melting furnace (Personal archive, 2020)

4.2.4 Spalling

Spalling from the surface, unrelated forces not inherent in refractory materials. It is defined as the losses generated by refractory. Those spalls can be caused by:

- Thermal stress happened by sudden changes in temperature,
- Located in the service position, formed between the original surface and the modified surface structural stress and stress created by mechanical forces,
- Forces created from internal vapor pressure (Banarjee, 1998).

4.3 Investigation Of Refractory Failure Mechanisms In Aluminum Industry

Most reactions occur at metal level where solid refractory, molten metal and gases are in triple form. Corundum formation on the refractory wall above the metal level causes stress spalling of the refractory. The refractory wall above the corundum pile is only in contact with gases from the melt (Hemrick et al., 2008). In fact, although corundum formation prevents the acceleration of corrosion at first, corrosion continues as a result of spalling and turbulence in the melt. Corundum formation also reduces the furnace usage volume (Brondyke, 1953). Spills and cracks in bricks during corrosion are largely attributed to these volumetric expansion reactions that occur in

the refractory (Siljan et al., 2002). The type and quality of the refractory are extremely important for limited metal penetration.

4.4 Refractory Wear Mechanisms In Aluminum Melting Furnaces

There are 3 factors effecting the-refractory wear in aluminum melting and holding furnaces.

- Reaction between molten aluminum and refractory material
- The interface reaction between the refractory material and the upper atmosphere and molten aluminum
- The reaction between the volatiles in molten aluminum and the refractory (Allaire, 2000).

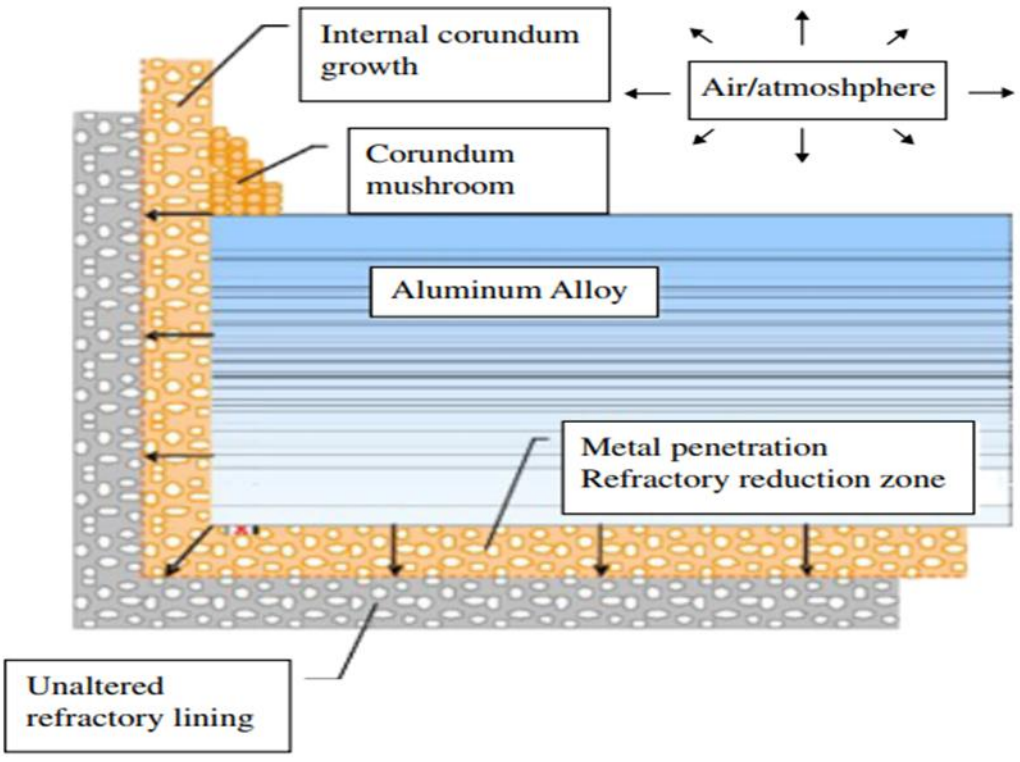

Figure 4.2 Schematic of corrosion and wear mechanisms associated with aluminum contact refractories (Hemrick et al., 2008)

Figure 4.2 demonstrates corrosion mechanisms within the regions (Hemrick et al., 2008)

1. Direct oxidation
2. Direct oxidation and reduction of silica
3. Reduction of silica

The reaction type for these mechanisms is given above and below (Allaire, 2000):

– Direct Oxidation

$$2\ Al + 3/2\ O_2 \rightarrow Al_2O_3 \quad (4.1)$$

– Reduction of Silica

$$2\ Al + 3/2\ SiO_2 \rightarrow 3/2\ Si + Al_2O_3 \quad (4.2)$$

4.4.1 Interaction Between The Molten Aluminium And Refractory

Requirements for refractories in aluminum melting and holding furnaces is:

– It should not react with molten aluminum.
– It should have a low solubility in the molten aluminium.
– It should not react with Al_2O_3 in the slag.
– It should have low thermal conductivity.
– It must have hydration resistance (after melting the fuel after melting it is important because of its high content of water vapor).
– It must have resistance against oxidation.
– It should be stable up to 1200 ^oC (rich in oxygen in burners may be higher if air is used).
– It should have good mechanical strength

With a strong reductive environment aluminum is infiltrated in to the refractory and which causes wear. The mechanism of this wear is as follows:

1. On the surfaces of refractories in contact with molten aluminum, an interface reaction occurs, "wetting" behavior occurs.
2. The molten aluminum refractory is penetrated into the interior through the open pores in the body. The sizes of the pores affect the penatration of the molten aluminum; This behavior changes with temperature, refractory composition,

structure (especially the surface structure) and the composition of the molten metal.

3. There is a chemical reaction between refractory and molten aluminum. Glassy phases such as silica and silicates in the brick are reduced and transformed into metallic silica, and alumina is formed as another component with these reactions.
4. Aluminum infiltration increases with the formation of metallic silica (the melting temperature of the metal bath decreases) and this creates a thickening bad layer.
5. This deteriorating layer expands more in volume than the refractory itself, and this causes the loss of the structure with temperature fluctuations.
6. There are spills on the refractory surface with the continuity of penetration.
7. Corrosion in refractory continues and progresses with melt aluminum infiltration (Banarjee, 1998).

It might be concluded that aluminum infiltration could be prevented by the following two methods when the above mechanisms are examined carefully:

1. Microstructural prevention of penetration (in terms of porosity and pore diameter)
2. Decreasing the wettability of the refractory by molten aluminum and reducing reaction with refractory (providing thermodynamic stability in refractory)

4.4.2 Interface Reactions Of Refractories With Molten Aluminum And Atmosphere

Alumina forms on the refractory surface oxidized in the upper atmosphere by penetrating aluminium into the refractory. Any number of microcrack results in surface depending volume chance of alumina formation (Banarjee, 1998).

4.4.3 Reactions Of Refractories With Volatile Matters In Molten Aluminium

Generaly, alkali salts (chlorides and fluorides of Na, K) are added in to the molten metal in order to avoid bath oxidation and to remove the impurities. These fluxing agents are very forceful chemically and tend to react with the refractory producing low melting compounds and vapours, subsequently increasing the corrosive tendency of

themelt (Pereira & Baldo, 1997). Moreover, alkalies also trigger and enhance the corrosion reactions, resulting in additional contamination of the metal with alkaline metals. Conventionally, aluminium metal from a reduction cell is known to have sodium concentrations in the order of 100 ppm, while in holding furnaces, the levels are further low with 10-20 ppm order (Furness & Pygall, 1983).

4.5. Reduction Of Oxides By Molten Aluminium-Refractory

4.5.1 Reduction Of Oxides In Aluminium Bath

The reduction of oxides plays an important role in refractory. Aluminum reduces less stable oxides (Allaire, 2000).

Table 4.1 summarises the free energy transformations involved in the reduction reaction of aluminium metal with oxides usually found in refractories. From the table, itisclear that aluminium cannot reduce the oxides of Mg, Ca and Ba since the reactions have a positive free energy change. This could explain the reason for proposed usage of Mg, and Ba based compounds as non-wetting additives to monolithics (Allaire, 2000) (Siljan et al., 2002).

Table 4.1 Calculated Gibbs Energy for reactions between refractory oxides and molten aluminium metal at selected temperatures (Allaire, 2000)

Reactions Studied	**Gibbs Energy (kJ/mol)**		
	(523°C)	**(923°C)**	**(1323°C)**
$4Al + 3SiO_2 \rightarrow 2Al_2O_3 + 3Si$	- 553.4	- 503.1	- 444.6
$4Al + 3ZrO_2 \rightarrow 2Al2O_3 + 3Zr$	- 15.6	23.9	69.4
$2Al + 3MgO \rightarrow Al_2O_3 + 3Mg$	119.8	114	40.5
$2Al + 3CaO \rightarrow Al_2O_3 + 3Ca$	229.9	234.3	174.6
$4Al + 3TiO_2 \rightarrow 2Al_2O_3 + 3Ti$	- 455.7	- 408.4	- 358.2
$2Al + Cr_2O_3 \rightarrow Al_2O_3 + 2Cr$	- 498	- 469	- 437.7
$2Al + 3ZnO \rightarrow Al_2O_3 + 3Zn$	- 615.7	- 621.2	- 732.4
$2Al + Y_2O3 \rightarrow Al_2O_3 + 2Y$	246.1	263.4	284
$8Al + 3Al_6Si_2O_{13} \rightarrow 13\ Al_2O_3 + 6Si$	- 1101.8	- 965.3	- 816

4.5.2 Reduction Of Silica (SiO_2)

The systematic investigation of the interfacial behaviour of the Al-alloy with refractories containing varying Al_2O_3-SiO_2 levels appeared that the major mechanisms in the interfacial reactions were corundum formation and SiO_2 reduction (Koshy, 2009).

In industry, aluminum is often used with metals such as Si and Mg by alloying in order to lower the melting temperature of the alloy. MgO is formed immediately. Since it is more stable Al_2O_3 in its alloys -especially Al-Mg alloys-. Wetting is achieved in the refractory interface and reduction of silica following reactions occur by the way of alloying (Oliveira et al., 2002).

$$4Al(l) + 3SiO_2 \rightarrow 2Al_2O_3(s) + 3Si(l) \quad (4.3)$$

$$8Al(l) + 3(3Al_2O_3.2SiO_2)(s) \rightarrow 13Al_2O_3(s) + 6Si(l) \quad (4.4)$$

Silica is generally found in refractories in 3 forms: natural silica, mullite in the form of silicates and micro silica. Mullite reacts with molten alumina as can be seen equation 4.4.

4.5.3 Reduction Of Mg And Zn Metals In Al-Alloy

Mg metal in aluminium alloys constitutes the first refractory-alloy reactions. Magnesium is a highly reactive metal and it does the initial reduction of some oxides in the refractory. Furthermore, it makes the refractory structure more vulnerable to aluminum attack (Koshy, 2009). If molten magnesium and zinc present, refractory deteoriation is high (Allahevrdi et al., 1998).

Thermodynamically, initial Mg infiltration would reduce alumina and Al and Magnesium Oxide (MgO) forms illustrated equation 4.5. The latter further reacts with alumina in refractory to create Mg-Spinel ($MgAl_2O_4$) illustrated in 4.6. Thats the reason of Mg-rich regions. Spinel formation causes about 8% volumetric expansion, which is due to the expansion stress and spillage.

$$3Mg + Al_2O_3 \rightarrow 3MgO + 2Al \ (\Delta G = -66.14 \text{ kJ}) \quad (4.5)$$

$$MgO + Al_2O_3 \rightarrow MgAl_2O_4 \ (\Delta G = -33.36 \text{ kJ}) \quad (4.6)$$

Mg rich regions could also possibly be aggregates of MgO and Al_2O_3 crystals, instead of spinel $MgAl_2O_4$. But, both MgO and Mg-spinel are thermodynamically stable, such that these phases resist to further reaction with Al metal due to the greater affinity of Mg to oxygen (Koshy, 2009).

MgO and Mg spinel which is the latter product in the Al alloy / Al_2O_3 system may not be reduced by Al metal and reactions may stop. But Mg silicate phase in Al alloy / SiO_2 system can be reduced by Al metal demonstrated in 4.15. Possible reactions below 1523 K (1250 °C) free energies of formation were given following equations (Koshy, 2009):

$$2SiO_2 + 3Al_2O_3 \rightarrow Al_6Si_2O_{13} \ (\Delta G_{1523K} = -22.0 \text{ kJ}) \quad (4.7)$$

$$3Al_2O_3 + 2SiO_2 + 13Mg \rightarrow 13MgO + 6Al + 2Si \ (\Delta G_{1523K} = -568.735 \text{ kJ}) \quad (4.8)$$

$$SiO_2 + 2Mg \rightarrow 2MgO + Si \ (\Delta G_{1523K} = -196.16 \text{ kJ}) \quad (4.9)$$

$$SiO_2 + MgO \rightarrow MgSiO_3 \ (\Delta G_{1523K} = -30.96 \text{ kJ}) \quad (4.10)$$

$$4Al + 3SiO_2 \rightarrow 2Al_2O_3 + 3Si \ (\Delta G_{1523K} = -456.20 \text{ kJ}) \quad (4.11)$$

$$MgO + Al_2O_3 \rightarrow MgAl_2O_4 \ (\Delta G_{1523K} = -33.36 \text{ kJ}) \quad (4.12)$$

$$3Mg + Al_2O_3 \rightarrow 3MgO + 2Al \ (\Delta G_{1523K} = -66.14 \text{ kJ}) \quad (4.13)$$

$$2SiO_2 + 2Al + Mg \rightarrow MgAl_2O_4 + 2Si \ (\Delta G_{1523K} = -326.18 \text{ kJ}) \quad (4.14)$$

$$4MgSiO_3 + 4Al \rightarrow 2MgAl_2O_4 + 3Si + Mg_2SiO_4 \ (\Delta G_{1523K} = -458.06 \text{ kJ}) \quad (4.15)$$

In this case, the reaction will continue until the alloy or refractory is exhausted. Silica reduction will cause volume reduction in the body (Koshy, 2009)

4.6 Factors Affecting Refractory Corrosion In Al-Casting

The corrosion resistance of refractories is strongly dependent on its physical and chemical properties which in turn are dependent on the process temperature. The metal

penetration into the refractory is believed to be strongly impacteed by the physical and chemical properties of the refractory as well as the working temperatures (Brondyke, 1953).

The major physical properties which influence corrosion behaviour include:

- Porosity of the refractory.
- Effect of particle size distribution.

The major chemical properties that contribute towards refractory corrosion are:

- Composition of the refractory.
- Presence of crystalline/mineral phases
- Presence of non-wetting additives

4.7 Typical Failures In Melting Of Aluminum

Refractory efficiency is usually high in shaft type furnace. The shaft type melting furnace serve for several years without repair. The two zones must be constantly protected in the furnace line for long furnace life. The first of these regions is edge walls located in metal level. The second is floor and mud formation is matter of floor. This positioning of muds lowers capacity of furnace.

CHAPTER 5
HIGH ALUMINA REFRACTORIES AND RAW MATERIALS

5.1 High Alumina Refractories

The basic raw materials of high alumina refractories are purified molten corundum produced by electro melting or sintering. Silimanite group minerals are kyanite, andalusite and sillimanite. Silimanite group minerals transforms into mullite and crystallite, when they undergo a mineralogical change with heat treatment. It is possible to produce bricks of this class with a single binder (usually 5-15% bonding clay) and with a small amount of various chamotte raw materials with high alümina content (Routschka, 1997).

In high alumina bricks, improving of properties such as thermal shock resistance, corrosion resistance is possible with the addition of materials such as zircon, titanium oxide and graphite. If the proportions of these materials exceed 5%, they are considered as special groups (Routschka, 1997).

Classification and coding of bricks produced according to raw material types are given in Table 5.1 (Routschka, 1997).

Table 5.1 Classification of high alumina refractories (Routschka, 1997)

DIN EN 12475-1		Iron and Steel Materials Document 912			
Alumina-silicate refractories	Corundum refractories	Bauxite refractories	Silimanite refractories	Mullite refractories (fused sinter)	Mullitted material refractories
≥ 98 Al_2O_3	HA 98				
95≥ Al_2O_3<98	HA 95				
85≥ Al_2O_3<95	HA 85	B 85			
75≥ Al_2O_3<85	HA 75	B 80	SK 75	EK 80	
65≥ Al_2O_3<75	HA 65	B 70	SK 65	E70/M70	
55≥ Al_2O_3<65	HA 55	B 60	S 55	M 60	TM 55
45≥ Al_2O_3<55	HA 45	S 50	A 50, A 55		

Refractories classified as firebrick (clay based) have the ratio maximum 38- 40 % alumina. As well as silicon, andalusite and kyanite refractories can contain 50- 60 % alumina. Calcined (burned) bauxite is used in materials with 80- 85 % Al_2O_3 content. Calcined or sintered (tabular) alumina produced by the synthetic way or Bayer is used for higher alumina content (Schact, 2004).

Table 5.2 Chemical and physical properties of bricks containing 50 %- 60 % Al_2O_3 (Schact, 2004)

Classification	% 50 $A1_20_3$ clay based	% 50 Al_2O_3 Bauxite based	% 60 Al_2O_3 clay based	% 60 Al_2O_3 Bauxite based	% 60 Al_2O_3 Andalusite based
$A1_2O_3$	50.5	49.5	58.1	62.1	58
SiO_2	44.5	49.5	38.2	32.5	39
Fe_20_3	1.3	1.3	1.2	1.2	1.5
TiO_2	2.3	2.5	2.2	2.6	0.2
Alkalis	0.8	0.7	0.1	0.8	<0.3
Bulk Density (gr/cm_3)	2.38-2.45	2.37	2.52	2.50-2.59	2.55
Apparent porosity %	11-16	17.5	14.3	17-20	<15
CCS, Mpa	48-69	28-55	58	34.5-62	

Chemical and physical properties of alumina-silicate bricks are given depending on the alumina content and the main raw material class used in Table 5. 2 and 5.3 (Schact, 2004).

Table 5.3 Chemical and physical properties of bricks containing 70%- 85% Al_2O_3 (Schact, 2004)

Classification	%70 Al_2O_3 Bauxite based	Mixture of Calcine bauxite/clay	%80 Al_2O_3	%85 Al_2O_3
$A1_2O_3$ SiO_2 Fe_20_3 TiO_2 Alkalis Bulk Density (gr/cm_3) Apparent porosity % CCS, Mpa	71.8 22.9 2.3 0.2 0.3 2.51 21.0 57.6	70.1 23.6 2.0 3.0 0.3 2.60 20.0 38-65	79.9 13.6 1.2 3.6 0.6 2.72-2.82 15-18 48-69	84.1 7.3 1.1 2.6 0.2 2.82-2.92 14-17 83-110

5.2 Al_2O_3-SiO_2 Phase Diagram

Alumina-silicate refractory technology can be literally improved by examining the Al_2O_3-SiO_2 phase diagram. When the Al_2O_3-SiO_2 phase diagram in Figure 5.1 is examined, three basic formations will appear. These:

1. When we consider that the mixture of alumina and silica is heated, as a reaction product mullite will be formed ($3Al_2O_3.2SiO_2$). Theoretical composition of mullite consist of 71.6 % Al_2O_3 and 28.4% SiO_2. Mullite has a high refractoriness, it melts at 1850 °C. When the alumina content in the composition approaches 72% refractoriness increases. Close to the theoretical composition of mullite, a mullite solid solution (marked “mullite ss”) forms.

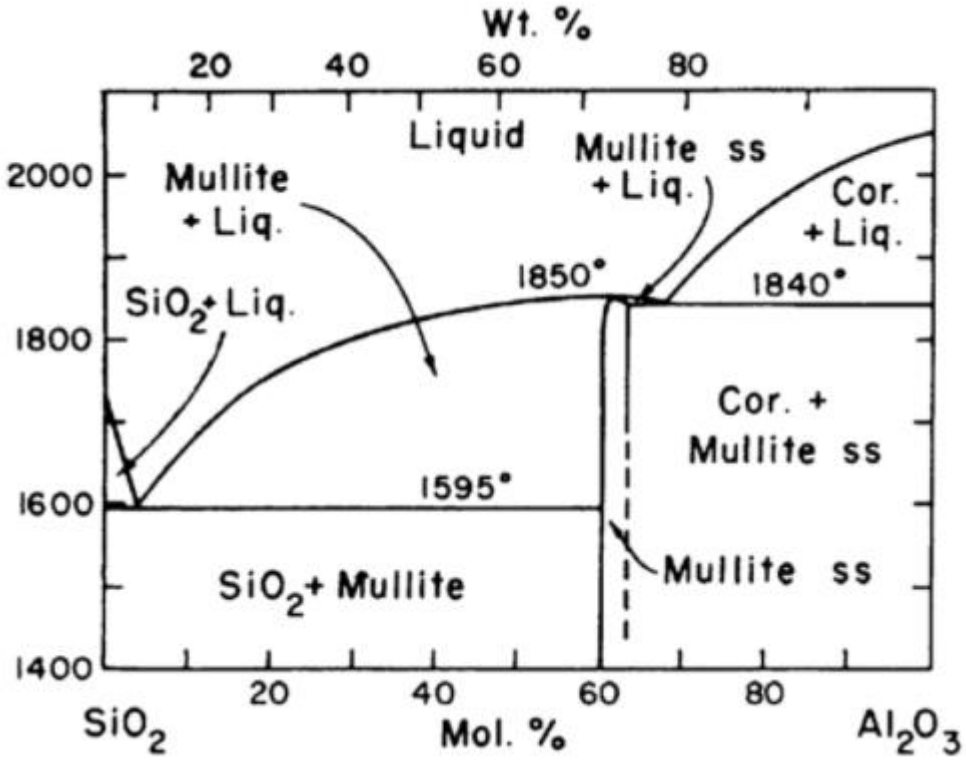

Figure 5.1 The Al_2O_3-SiO_2 (Alumina-Silica) phase equilibrium diagram (Schact, 2004)

1. Figure 5.1 has a solidification curve at 1595 ° C. SiO_2 decreases from 100 percent SiO_2 (between SiO_2 and mullite binary eutectic)- solid phases (cristoballite or glass and mullite) exist up to 72 weight % Al_2O_3, until 1595 °C is surpassed. Above 1595 °C, refractory material in this composition will form a liquid phase or melt. The word glass indicates the presence of a state of vitreous and noncrystalline.
2. Above 72% Al_2O_3, the solidification curve settles at 1840 °C and it continues until it has a 100 % alumina content. Below 1840 °C, melting is not observed and the refractoriness increases as the alumina content increases in the diagram. Corundum has a melting point of around 2050 °C.

Table 5.4 Alumina-silicate bricks and equilibrium phases as regards qualities (Schact, 2004)

Al_2O_3 range in most standards	Common phases	Types of production
Less than %50 Al_2O_3	Fireclay (Chamote) Phases on phase diagram: mullite and glass (can contain free SiO_2)	Usually made from %100 fireclay
%50-60 Al_2O_3	Sillimanite, andalusite and kyanite Phases on phase diagram: Major phase- mullite and Minor phase- glass (can contain free SiO_2)	Made from %60 Al_2O_3 minerals and contain some fireclay
%70 Al_2O_3	Mullite Phases on phase diagram: Major phase- Mullite. Products made with bauxite contain corundum, mullite and glass.	Made either from bauxitic clay or calcined bauxite and clay
%80 Al_2O_3 %85 Al_2O_3	Bauxite Phases on phase diagram: Major phase- Corundum. Minor phase- Mullite and glass	Made from calcined bauxite
%90 Al_2O_3	Alumina Phases on phase diagram: Major phase- Corundum.	Made from tabular and/or fused synthetic (Bayer process) alumina aggregates

Oxide (flux oxides- usually alkali oxides) amount that varies according to the raw materials are an important issue that changes all structural properties in alumina-silicate refractories. Table 5.4 shows Alumina-silicate bricks and equilibrium phases as regards qualities.

Alkalies are present as sodium oxide (Na_2O) and potassium oxide (K_2O) In natural clays. Both of these strong fluxes have an effect on their performance in service. CaO, FeO, Fe_2O_3 and TiO_2 also present in structure. More flux generally means more glass will be existing in fired refractory. It is the reason why–fireclay bricks specifically, exhibit improved service efficiency as bigger spalling resistance. If they involve lower levels of flux in other words bigger mullite content they exhibit increased spalling resistance. Bigger glass content decreases spalling resistance.

Increasement in mullit formation cause decreasement in glassy phase depending on the refractoriness, and melting degree increases, as the Al_2O_3 ratio increases (Schact, 2004).

5.3 Raw Materials

5.3.1 White Fused Alumina (WFA)

WFA (White fused alumina obtained by melting of calcined alumina at 2040 ° C in an electric arc furnace. Although being pure form of fused alumina, WFA products are of high porosity and low volumetric density. WFA has high refractoriness and wear resistance and is chemically inert (Banarjee, 1998). Table 5.5 presents chemical and physical property limit values for WFA.

Table 5.5 Chemical and physical property limit values for WFA (Banarjee, 1998)

Type	Main component	Rate of impurity % wt.	Crystal System	Crystal dimension (μm)	Bulk density (gr/cm3)	Apparent porosity (%)	Refractoriness (SK)
White Fused Alumina (WFA)	Al_2O_3 ≥ 99.5	$Na_2O \leq 0.3$ $SiO_2 \leq 0.1$ $Fe_2O_3 \leq 0.1$	Corundum Trigonal	A few thousand	3.5 – 3.7	5 – 10	> 40

5.3.2 Titanium Dioxide

Titanium oxides commonly present in high alumina refractory compositions are as impurities from bauxite. Existence of titania leads to increased densification due to the

formation of glassy aluminium titanate phase. Also, at higher temperatures liquid phase sintering results in the formation of aluminium titanate (Volceanov et al., 2004). However, titania is depleted by aluminium metal resulting in metal contamination (Sobczaketal.,2004). Some mineral phases in the formation of mullite, such as iron oxide and titanium, serve as mineralizers (Johnson & Pask, 1982). Figure 5.2 shows Al–Ti binary phase diagram (Sun et al., 2019).

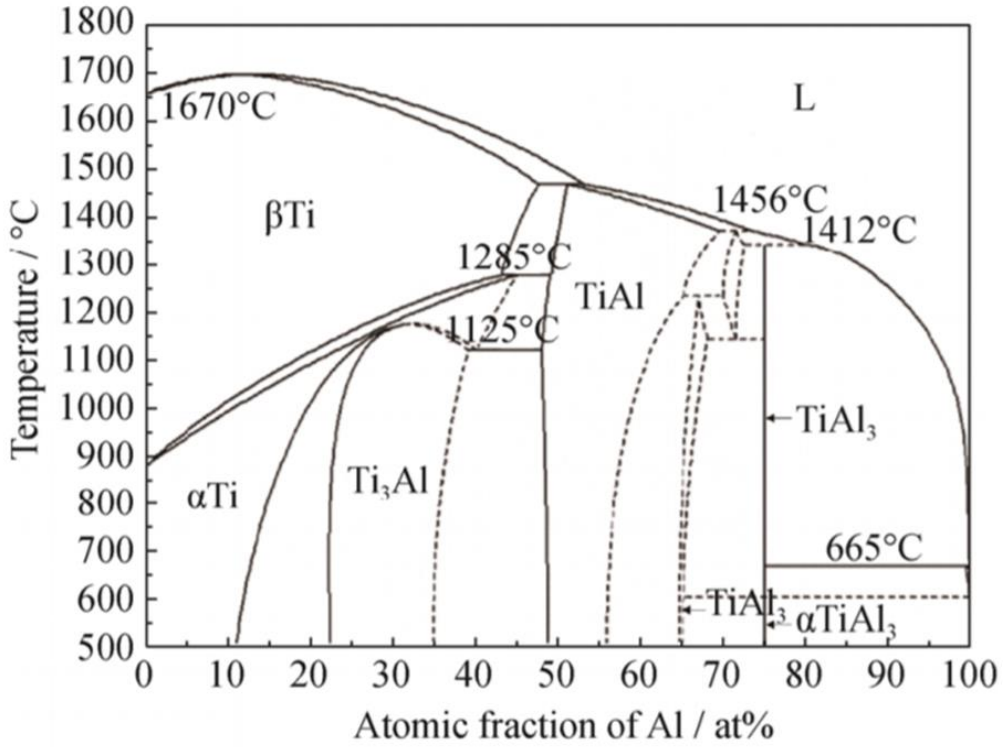

Figure 5.2 Al-Ti binary phase diagram (Sun et al., 2019)

Aluminium titinate (Tialite) is a stoichiometrical compound out of A_2O_3 and TiO_2 which is not stable until reaching 1200 ^oC. Below this temperature, that is up to 800 ^oC, tialite decomposes into the original constituents.

The manufacture of tialite materials is based on very fine grain raw materials. Tialite forms during sintering or in the preceding fusion or reaction processes.

Tialite is distinguished by very little thermal expansion and, consequently, excellent thermal shock resistance. The strength is low for a fine ceramic material. Tialite has poor wettability in contact with non ferrouus melts like aluminum.

The mentioned properties of tialite are used specifically for casting equipment when melting non ferrous metals.

5.3.3 Graphite Carbon

Carbon element is found in nature in the form of diamonds, graphite and coal. For refractory process graphite is important for the production of carbon bricks. Differences of carbon and graphite refractories lies on the basis of their crystal structure. Graphite refractories show layered structure, whereas carbon refractories usually do not show a well- ordered crystalline structure. Figure 5.3 shows base material pyramid with the location of the refractory materials (Routschka, 2008). Figure 5.4 shows crystal structure of graphite (Ewais, 2004).

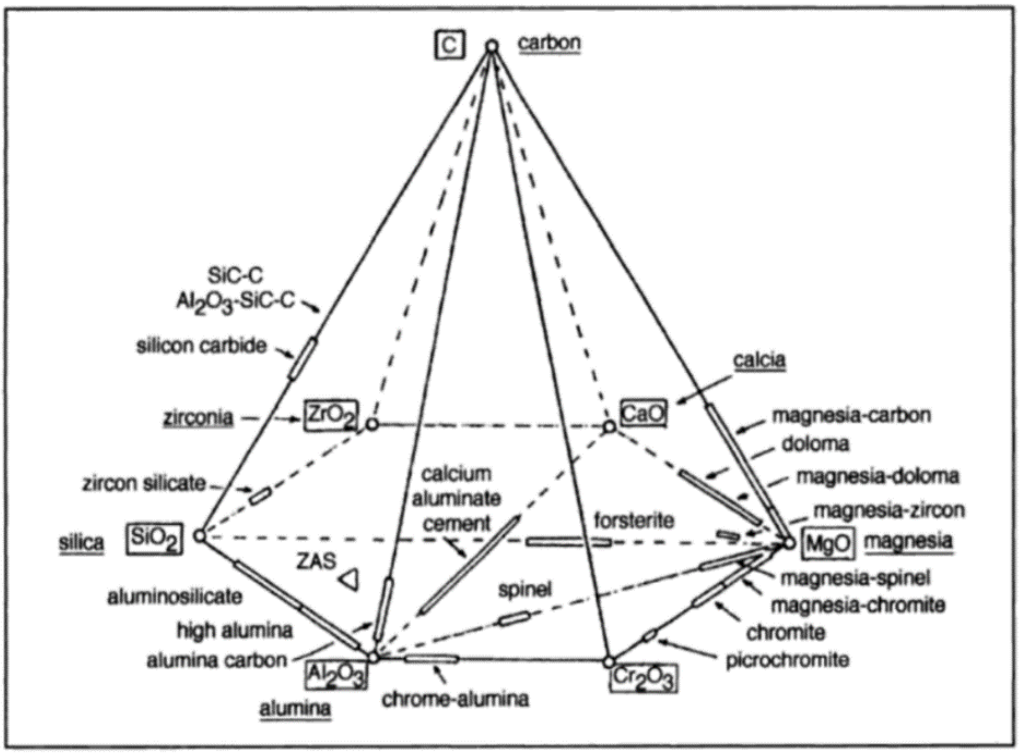

Figure 5.3 Base material pyramid with the location of the refractory materials (Routschka, 2008)

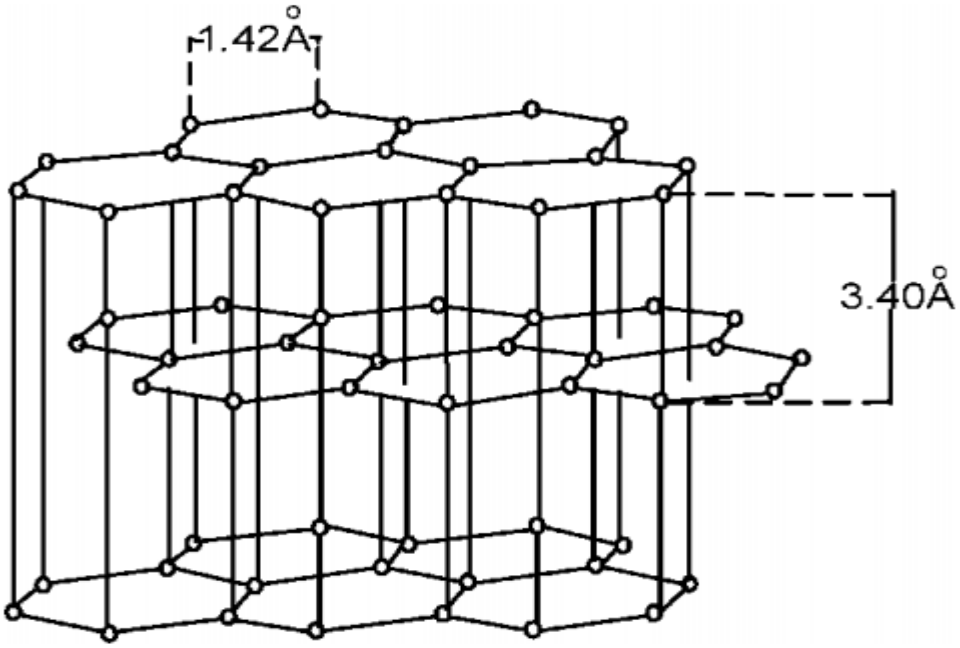

Figure 5.4 Crystal structure of graphite (Ewais, 2004)

Carbon cantaining refractories find application iron- steel industry generally due to their non-wetting properties. However, The common problems with carbon containing refractories are their poor oxidation resistance and low mechanical strength. To improve the oxidation resistance, special techniques as of antioxidant addition technique has been established.

The antioxidants, often involving metals/ alloys, carbides and boron containing compounds, can protect graphite/ carbon from oxidation via two major mechanisms. (Shaowei Zhang, 2007). Antioxidants originally employed for oxidation resistance were also found to show some reinforcing effect (Yamaguchi, 1987). Metallic powders might be utilized as antioxidants, but that powder, e.g. aluminum, has a serious shortcoming due to extensive hydration and the release of explosive hydrogen gas. Zhang (2005) and Liu (2019) recently developed a promising technique for coating graphite with TiC, but still no report is available on the characteristics of castables prepared with such graphites. Yoshimatsu et al. (1995) studied coated graphite with alumina derived by an alkoxide precursor; however, only some reports are available on castables prepared with this alumina-coated graphite.

Juhasz et al. (2013) studied liquid aluminium which does not wet graphite**.** Motivated by this study, graphite addition was added into Al_2O_3 refratory mixture to obstruct wettability of carbon by liquid aluminum. In this thesis**,** graphite was added into refratory mixture starting from these studies' point of view.

CHAPTER 6
EXPERIMENTAL STUDIES

6.1 Introduction

In this study, it is aimed to investigate high alumina bricks with additives used in aluminium melting furnaces. Lab-scale studies and industrial studies were conducted, in order to discuss and evaluate the results in real conditions. Physical, chemical, mechanical, thermal tests were carried out as laboratory studies. The corrosion test were carried out as industrial study. Figure 6.1 shows the flow chart of the experimental studies.

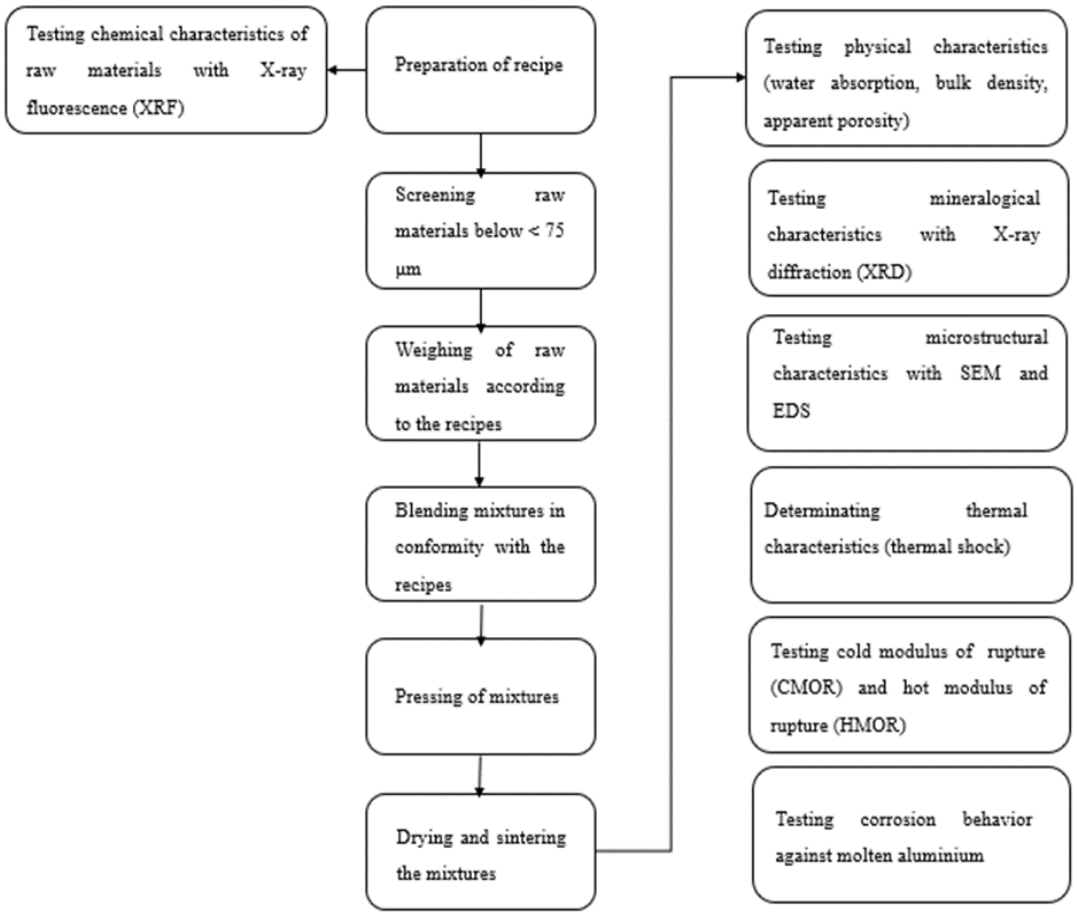

Figure 6.1 Flow chart of experimental studies

6.2. General Principles

6.2.1 Details With Experimental Instruments

- Porosity and bulk density tests were conducted in Seramiksan Turgutlu Ceramic Industry and Trade Inc.
- Energy dispersive X-ray fluorescence (EDXRF) of refractory powder and titania were analysed (Rigaku, Nex CG) at Chromatography and Spectroscopy Laboratorty in Ege University Central Research Test and Analysis Laboratory Application and Research Center.
- Three point bending strength values of the samples were determined (Ceramic Instruments, Strumento Mod. Mor/ 3- E, Scalo 0+40 Kg, Sassuolo, Italy) in Seramiksan Turgutlu Ceramic Industry and Trade Inc.
- Thermal shock resistance tests were conducted into furnace (Refsan, Kaleo27, Kutahya, Turkey) in Dokuz Eylul University.
- Scanning electron microscopy (SEM) of samples were analysed at Dokuz Eylul University Characterization Laboratory in Metallurgical and Materials Engineering Department with a scanning electron microscope (JEOL JSM 6060, Tokio, Japan).
- X-Ray diffraction patterns (XRD) picture were taken at Center for Fabrication and Application of Electronic Materials (Thermo Scientific, ARL X'TRA, Switzerland) in Dokuz Eylul University.
- Corrosion tests of samples were conducted into shaft type aluminium melting furnace (Enkotherm, TMT-2B 2000/1000, Istanbul, Turkey) at 820 °C in Volt Electric Motor Industry and Trade Inc.
- Three point bending strength at high temperature (HMOR) were determined in Kümaş Manyezit Industry and Trade Inc (Netzsch, 422 D/3, Selb, Germany).

6.2.2 Raw Materials And Their Pre-Treatmens

In this study, refractory powder (RP) was obtained from a company that supplies refractories. Initially, rough refractoy powder was ground for 10 min. by using ball mill (Tahya Makina, Türkiye). After grinding, and screening under 75 μm, fine powder were obtained. RP was screened at 100 rpm for 5 minutes by using a sieve shakers

(Retsch, AS200, Germany) in figure 6.3. Screened refractory powder under <75 μm is shown in Figure 6.2.

High Alumina powder (AP) obtained from a producer firm was not undergone to any treatment. As well as supplied graphite carbon (GCP) purity 99.0%, (Sinopharm Chemical Reagent Co. Ltd, Beijing, China) and titan dioxide powder (TP) supplied by Kimetsan, Turkey was not treated.

Figure 6.2 Pictures of (a) refractory powder (b) titania powder and (c) alumina powder (Personal archive, 2020)

6.2.3 Characterization Of Raw Materials

Refractory powder and alumina powder were chemically analyzed by X-ray fluorescence technique in a sequential wavelength energy dispersive spectrometer (XRF, Rigaku NEXCG). Table 6.1 and 6.2 shows chemical composition (% wt.) of alumina powder and refractory powder, respectively.

Table 6.1 Chemical analysis (XRF) result of alumina powder (AP) used as raw material

Constituents	XRF (wt. %)
Al_2O_3	99.60
ZrO_2	0.24
SiO_2	0.05
ZnO	0.02
CaO	0.01
Fe_2O_3	0.01

Table 6.2 Chemical analysis (XRF) result of refractory powder (RP) used as raw material

Constituents	XRF (wt. %)
Al_2O_3	63.90
SiO_2	18.60
CaO	5.26
BaO	4.81
SO_3	2.95
TiO_2	2.28
ZrO_2	0.90
Fe_2O_3	0.66

6.2.4 Preparation Of Recipes And Samples Production

Six different types of mixture were prerared. Additive free (only refractory powder) samples were also prepared for comparison. In order to analyse the effect of additives at different ratios, various amounts of AP, GCP, TP and compositions with each other were added in RP according to determined in table 6.3. Each mixture contained considerable enough quantity of material about 100 g, in order to produce refractory bodies The prepared refractory mixtures were wetted at 6 wt. % humidity. The

mixtures were then uniaxially compacted as rectangular prism and cylinder using hydraulic press machine (Sassuololab, Italy) under a pressure of 45 MPa. Samples were in the shape of a rectangular prism with 100 mm x 50 mm x 10 mm size, 150 mm x 25 mm x 25 mm size, 80 mm x 80 mm x 65 mm and in the shape of cylindrical shape with 50 mm x 50 mm size. The obtained samples of pressed mixtures were dried first in the open air for 72 h and afterward in the oven at 110 ◦C for 48 h for dehumidification. Dried samples were fired in laboratory-type electirical furnace shown in Figure 6. 4. Afterwards, the samples were fired at the rate of 5 ^{o}C/ min until 1200 ^{o}C for 2 hours. The fired samples were cooled down in furnace. Figure 6. 5 shows overview of refractory brick preparation process as a summary.

Figure 6. 3 Furnace using of sintering samples (Personal archive, 2020)

Table 6.3 Composition of the prepared samples, (weight %)

Codes	Identification	Explanation	Content (wt%)			
			RP	AP	GCP	TP
RP	Additive-free	Contains only RP	100	-	-	-
AP	Al_2O_3	Contains Al_2O_3 inside RP	90	10		
GCP	Graphite carbon	Contains Carbon inside RP	90	-	10	-
TP	TiO_2	Contains TiO_2 inside RP	99	-	-	1
AP:TP	Al_2O_3:TiO_2	Contains Al_2O_3 and TiO_2 inside RP	90	9	-	1
GCP:TP	Graphite carbon: TiO_2	Contains Carbon and TiO_2 inside RP	90	9	-	1

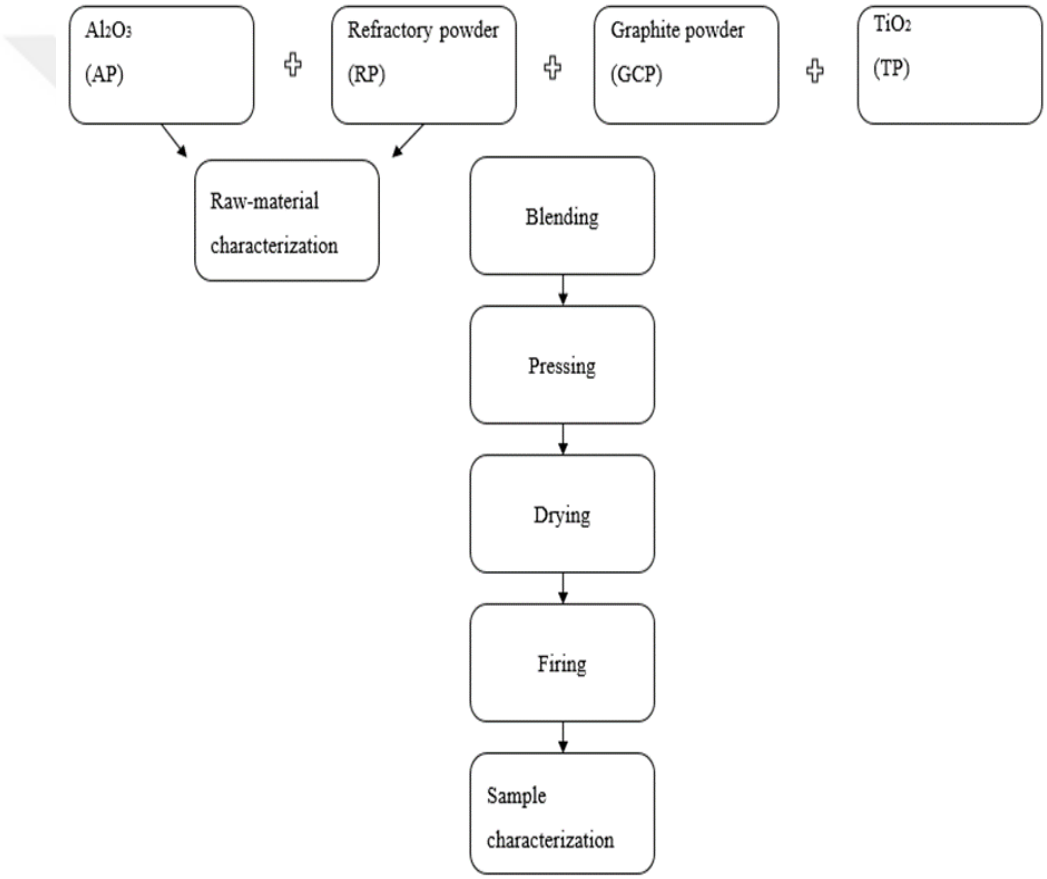

Figure 6.4 Overview of refractory brick preparation process

6.2.5 Characterization Of Samples

The apparent porosity, water absorption and bulk density of samples were evaluated through the Archimedes Principle. The determination of the mechanical strength was

performed at room temperature using the three point bending technique. Thermal test was conducted in a furnace. Samples were holded in chamber for 15 minutes at 950 ^{o}C and quenched.

The phase identifications for the fired refractories were performed by X-Ray diffractometry, with the aim to study the new phases formation after firing. SEM was used to analyse the interfacial microstructure of the fired samples. Corrosion tests were performed for the samples, in order to evaluate the additive effect on refractories.

6.3 Laboratory Experiments

- Physical properties of samples was tested according to archimedes principle using the standard ASTM C-20. Three samples were used for each composition.
- Cold modulus of rupture (CMOR) were performed using ISO 5014:1997 standard. The specimens' dimensions of bending part was 100 mm x 50 mm x 10 mm. Figure 6. 5 shows the cold modulus of rupture samples.

- Hot modulus of rupture (HMOR) were performed using ISO 5013 standard. The specimens' dimensions of bending part was 150 mm x 25 mm x 25 mm.
- Thermal shock test were applied according to DIN 5106. This standard offers applying heating temperature of 950 °C and then water quenching to a cylindrical test piece (50 mm × 50 mm). Figure 6. 6 shows the pressed thermal shock samples.
- Phase development of fired samples for each compositions was examined with XRD X-ray diffractometer (Thermo Scientific ARL X'TRA), using Cu Kα radiation with a wavelength, $\lambda = 1.54$ Å, in the 2θ-angle range from 10–90^{o}.
- SEM Microscopic imaging by SEM coupled with energy dispersive spectroscopy (EDS) were used to investigate the morphology, structure and composition of the materials. In this work, SEM imaging and analysis was done on a JEOL JSM 6060.

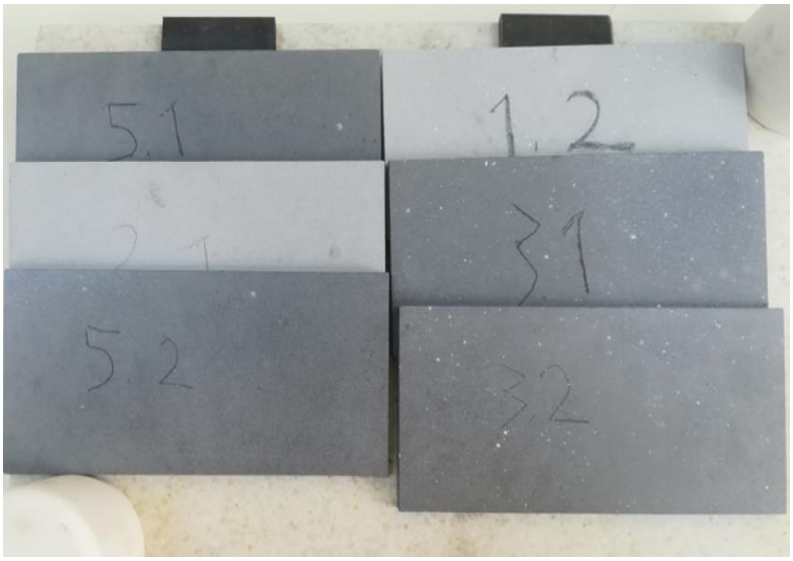

Figure 6.5 Cold modulus of rupture samples (Personal archive, 2020)

Figure 6.6 Pressed termal shock test samples (Personal archive, 2020)

6.4 Industrial Experiments

- For corrosion test crucible methodwas employed according to DIN 51069 standard. According to the DIN 51069 standard, 80x80x65 mm^3 square prism sample has a 40-42 mm of inner diameter and 35 mm of a cylindrical height cavity. Figure 6. 7 shows the corrosion test system. Figure 6. 8 shows followed stages for corrosion test. After completing test stages, cooled down samples were cut and their corrosion behaviours were examined. Penetration and corrosion investigations were made observational and compared with each other.

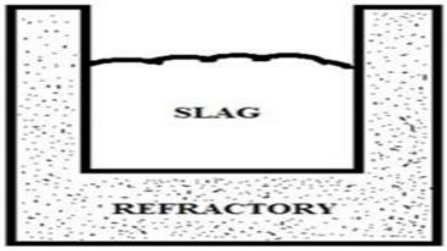

Figure 6.7 Slag methods crucible test

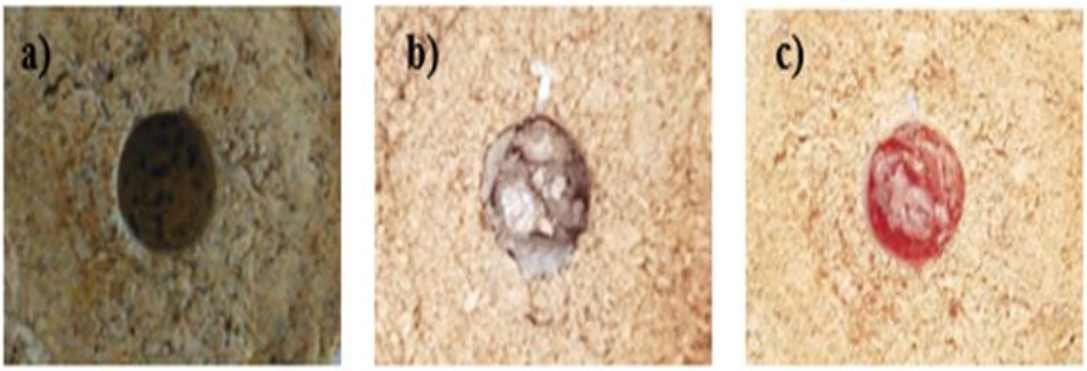

Figure 6.8 Followed stages for corrosion test a) drilled corrosion test sample; b) filled solid aluminium slag corrosion test sample; c) molten aluminium slag after corrosion test indicates, respectively (Personal archive, 2020)

CHAPTER 7
RESULTS AND DISCUSSION

7.1 Physical Tests

Obtained results for apparent porosity, bulk density and water absortion tests' results were shown in table 7.1. Samples without graphite additives have less apparent porosity thus their bulk densities are high. According to some other researchers high temperature oxidations of graphite lead to drastic deterioration due to graphite diminution, which lead pores in the samples (Ali Nemati & Moetakef, 2007). Moreover, the decrease in apparent porosity and hence water absorption the value of RP-TiO_2 is explained with the additional increase in the filling of spaces between bigger particles contained in the ceramic samples (Akintunde, Oyetunji, & Aramide, 2016).

Samples' porosity rate reached % 35.30 with graphite additive singly and up to % 37.35 with addition of graphite and TiO_2. However, singly TiO_2, alumina powder and both of them as an additive has been shown to have an effect on the porosity decreasement hereby low porosity, water absorption and highest bulk density. Formation of liquid phase of titania is the reason of low porosity according to reference sample.

Table 7.1 Results of apparent porosity, bulk density and water absorption tests

Codes of Samples	**Apparent Porosity (%)**	**Water Absorption (%)**	**Bulk Density (g/cm^3)**
RP	28.30	11.83	3.65
RP-AP	26.98	11.19	3.65
RP-TP	25.90	10.87	3.74
RP-AP-TP	25.00	10.17	3.78
RP-GCP	35.30	15.00	3.54
RP-TP-GCP	37.35	15.90	3.52

7.2 Thermal Shock Resistance Test

Thermal shock cycles were repeated until the test piece breaks into two or more large fragments and the table 7.2 represents the number of cycles. For thermal shock testing, samples were heated to 950 ^{o}C and air cooled. Test temperature is higher than temperature of molten metal region of aluminium melting and holding furnaces for complying with the DIN 5106 standard. Their average cycle numbers were evaluated. When the number of cycles is 30, the cycle is enough was seen and the experiment was concluded (Brochen et al., 2017). Table 7.2 presents the results of thermal shock resistance. RP-C and RP-TiO_2-C has lower than 30 since they were broken before 30 cycle number. Figure 7.1 shows the example of break into two pieces exposed cycle thermal shock.

Table 7.2 Results of thermal shock resistance

Codes of Samples	**Average Number of Cycles**
RP	30
RP-AP	30
RP- TP	30
RP-AP-TP	30
RP-GCP	20
RP-TP-GCP	22

Figure 7.1 Cylindrical test piece after thermal shock testing (Personal archive, 2020)

7.3 Cold Modulus Of Rupture (CMOR) Test

Table 7.3 shows prepared samples for CMOR test according to ISO 5014:1997. CMOR strength values of samples increase with alumina, alumina-titania and titania additive. Expected results were seen for alumina additive due to alumina and mullite phase abundance. Zhao et al. (2016) stated that titania phase improves strenght of alumina refractories. Also, titania phase improves strenght of alumina refractories slightly. Titania additives made bricks grain size reduction. This lead to increasement strenght of sample. Tialite phase also improved mechanical property.

Bending strenght decreased with respect to graphite additives samples in comparison with reference sample. It was corcerned that porous structure of samples with graphite was the reason for this decrasement.

Table 7.3 Cold modulus of rupture (CMOR) test results

Codes of Samples	**CMOR Strength (N/mm^2)**
RP	25.5
RP-AP	26.7
RP-TP	28.6
RP-AP-TP	31.5
RP-GCP	12.5
RP-TP-GCP	17.3

7.4 Hot Modulus Of Rupture (HMOR) Test

HMOR results of samples are shown in table 7.4. Yurkov (2015) reported the modulus of rupture usually decreases with temperature increasement due to increased viscosity of the glassy phases. This is because the values of HMOR were lower than CMOR in this study. Sample with graphite additives showed lowest strenghts in CMOR. Similarly, lowest strenghts were observed for samples with graphite additives in HMOR. The reason is that existance of any number of pores. The strength of RP-AP is higher than RP-TP, because the RP-AP has higher bonding strength with Al_2O_3. The result agrees with the report of Zhu et al. (2013). As for RP, samples without additive increased to the highest HMOR of 10.5 MPa.

Table 7.4 Hot modulus of rupture (HMOR) results

Codes of Samples	**HMOR Strength (N/mm^2)**
RP	10.5
RP-AP	7.7
RP-TP	6.7
RP-AP-TP	6.2
RP-GCP	6.2
RP-TP-GCP	5.8

7.5 Corrosion Test Results For Industrial Experiments

Figure 7.2 shows corrosion test results of samples. Siljan, Schoning & Grande (2002**)** asserted brick density, apparent porosity, gas permeability and pore size distribution play important role, but less influential roles on resistance of alumino-silicate refractories in the corrosion-test. This study appears to be in agreement with obtained result. Although physical properties of samples diverges with each other, their corrosion test results were not impressed with that properties. All samples without graphite resist to molten aluminium penetration.

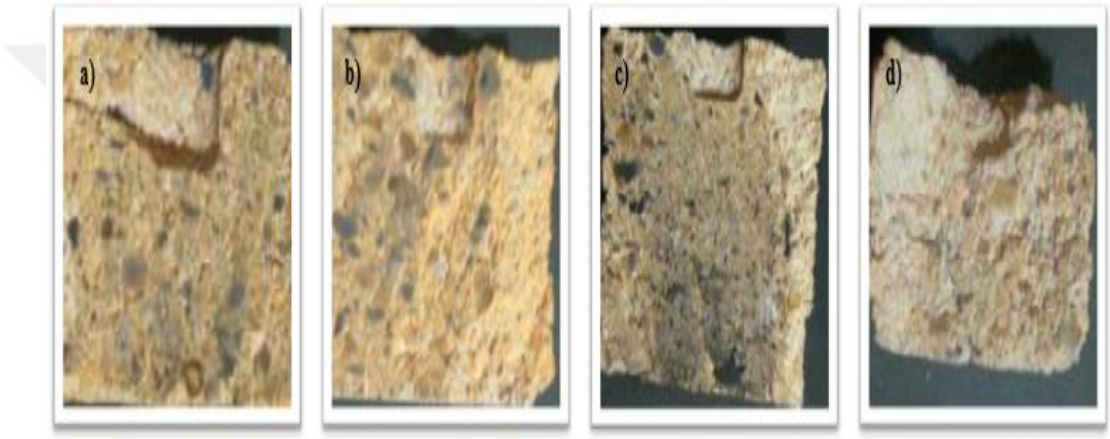

Figure 7.2 Cross sectional area view after corrosion test of a) sample without additive; b) sample with 10 wt. % Al_2O_3; c) sample with 1 wt. % TiO_2 and 10 wt. % Al_2O_3; d) sample with 1 wt. % TiO_2 indicates, respectively

Atzenhofer, Gschiel & Harmuth (2017) observed oxidation of carbon in their studies. It was also stated that refractories with carbon additives could suffer from oxidation. Thus, the structure of brick is destroyed and the slag can penetrate into the structure. This concept is supported by in this study, samples with graphite additives disintegrated while they were drilled. RP-GCP and RP-TP-GCP samples can not been investigated due to their collapse. Figure 7.3 shows the disintegrated sample with graphite additive.

Figure 7.3 Disintegrated corrosion test sample sample with graphite (Personal archive, 2020)

7.6 X-Ray Diffraction (XRD)

Figure 7.4 shows XRD graph of sample without additive after firing. Two main mineral phases exist in the sample without additive. These are corundum (Al_2O_3), mullite ($3Al_2O_3$:$2SiO_2$). The reference sample is mainly composed of mullite and alumina. Mullite spinel formed for all mixtures according to results. Furthermore, Al_2O_3 was found in each receipt according to result of X-Ray beam investigation.

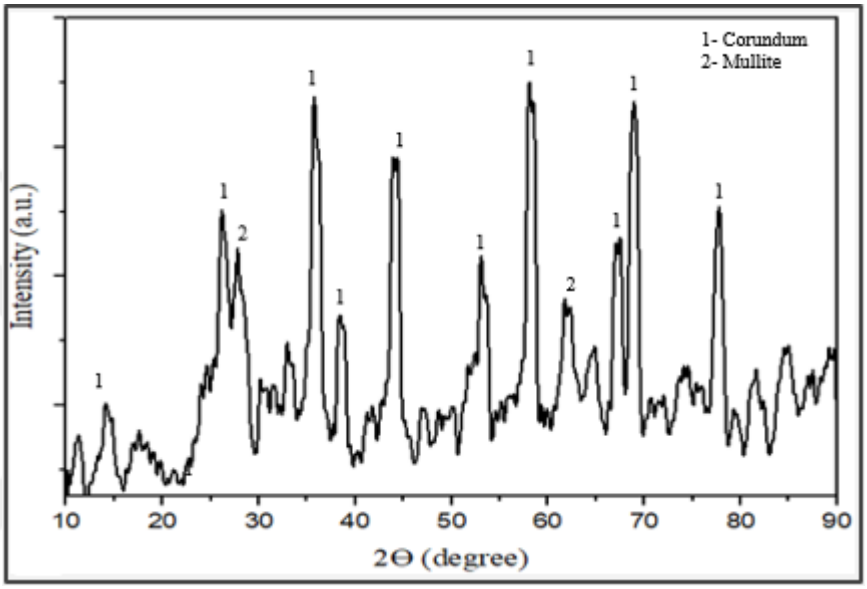

Figure 7.4 XRD patterns of sample without additive samples after firing (1-Corundum, 2-Mullite)

Figure 7.5 shows XRD graph of sample with 10 wt. % Al_2O_3 additive after firing. Compared with reference samples, peaks are more intense, especially with corundum and mullite phase.

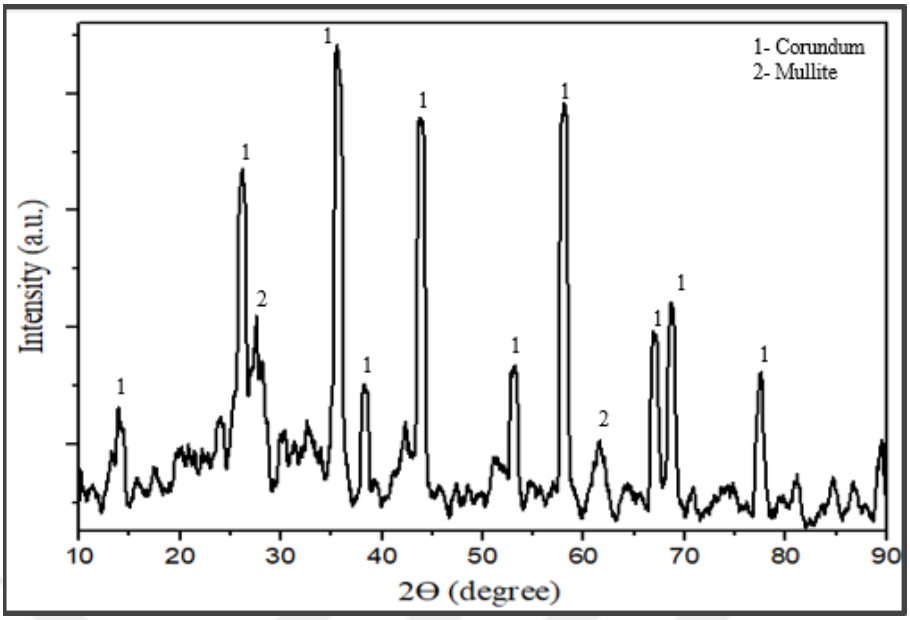

Figure 7.5 XRD patterns of sample with 10 wt. % Al_2O_3 additive samples after firing (1-Corundum, 2-Mullite)

Figure 7.6 shows XRD graph of sample with 1 wt. % TiO_2 after firing. As can be seen from the Figure, phase of titania with alumina occured as aluminium titanate (Al_2TiO_5). This phase is also called as tialite.

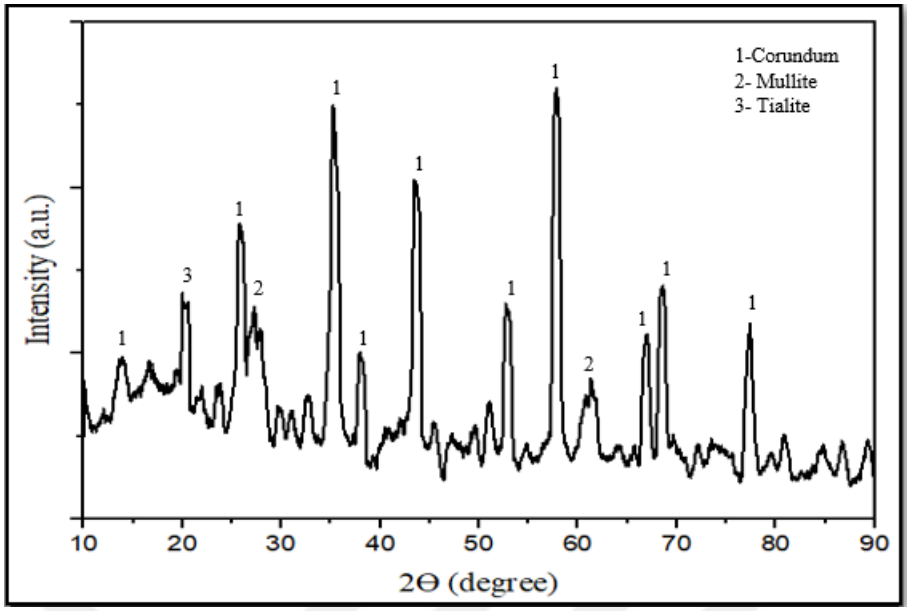

Figure 7.6 XRD patterns of sample with 1 wt. %TiO_2 additive after firing (1-Corundum, 2-Mullite, 3-Tialite)

Figure 7.7 shows XRD graph of sample with 1 wt. % TiO_2 and 10 wt. % Al_2O_3 after firing. Alumina additive samples indicate stronger intensity of corundum peaks as expected thermodynamically.

Relatively lower intensity of mullite peaks could attributed to the higher stability of the quartz phase, and higher activation energies and longer durations required for stable equilibrium phase formations. In addition, tialite phase was observed.

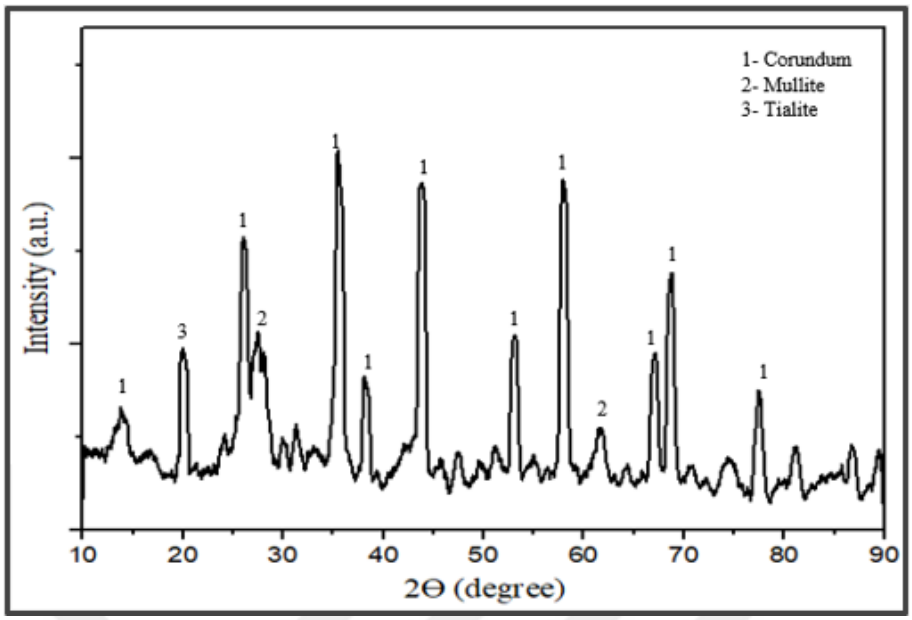

Figure 7.7 XRD patterns of sample with 10 wt. % Al_2O_3 and 1 wt. %TiO_2 additive after firing. (1-Corundum, 2-Mullite, 3-Tialite)

Figure 7.8 shows XRD graph of sample with 10 wt. % Graphite additive after firing. Peak on 23º indicates unshaped graphite structure (Mukhopadhyay et al., 2009). Lowness of the intensity of peak means disordered structure of graphite flakes. In addition, figure 7.9 shows XRD patterns of sample with 10 wt. % Graphite and 1 wt. % TiO_2 additive after firing. Similarly, disordered graphire phase are observed.

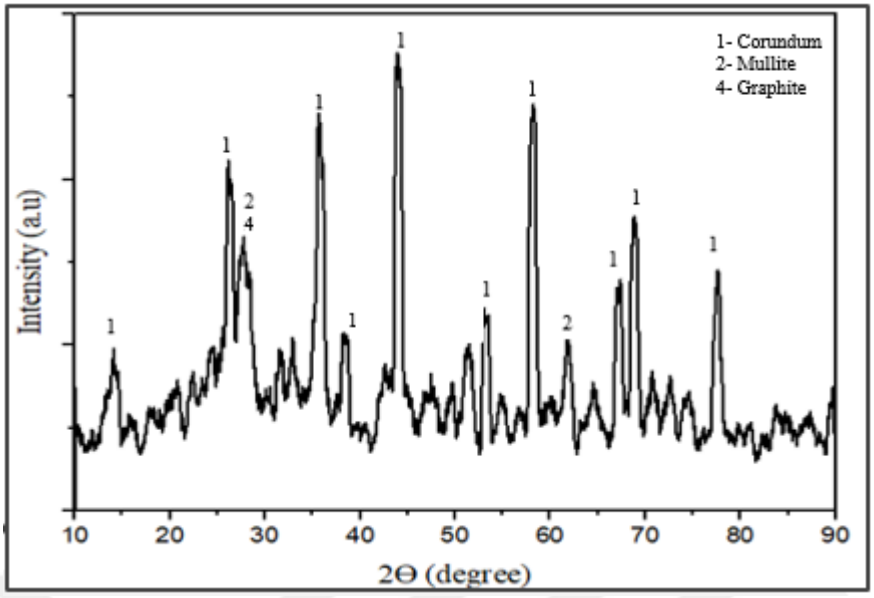

Figure 7.8 XRD patterns of sample with 10 wt. % Graphite additive after firing. (1-Corundum, 2-Mullite, 4- Graphite)

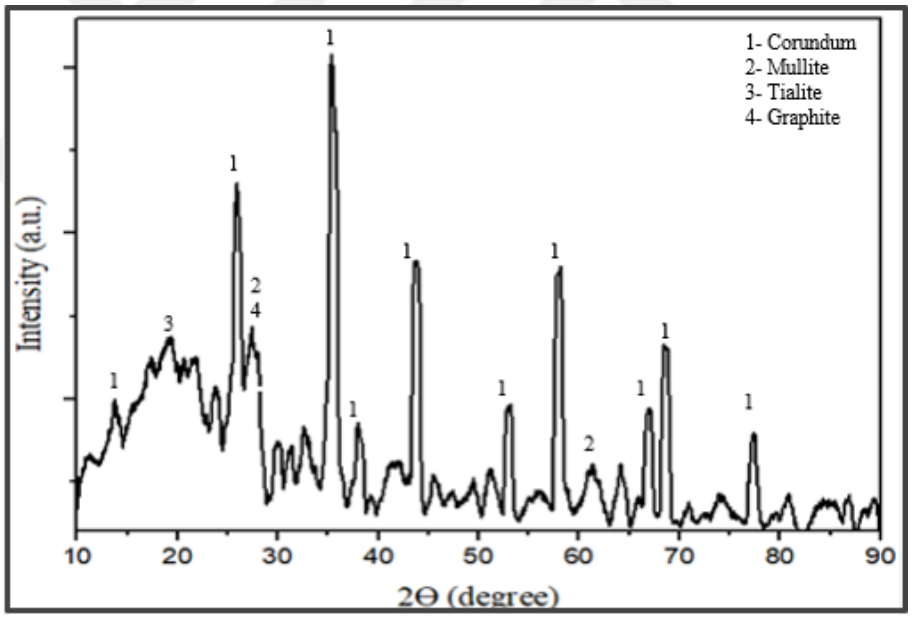

Figure 7.9 XRD patterns of sample with 10 wt. % graphite and 1 wt. % TiO_2 additive after firing. (1-Corundum, 2-Mullite, 3-Tialite, 4- Graphite)

7.7 Scanning Electron Microscopy (SEM)

Figure 7.10 shows microstructure of RP sample. The presence of capillary mullite phase was clearly seen. Figure 7.11 shows EDS analysis diagram of sample without additive after firing.

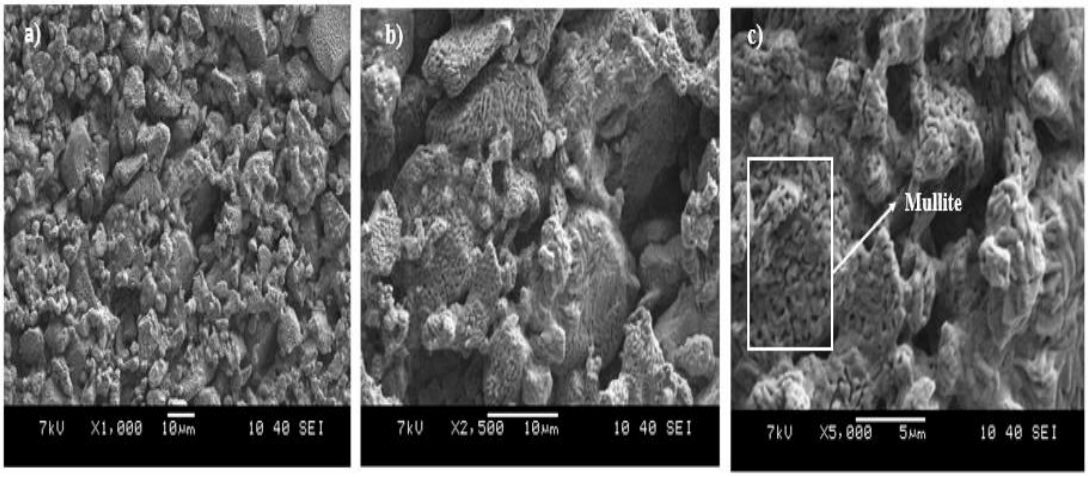

Figure 7.10 Scanning electron microscopy images of the region without additive after firing and analyzed EDS a) X1000; (b) X2500; (c) X5000 magnification indicates, respectively

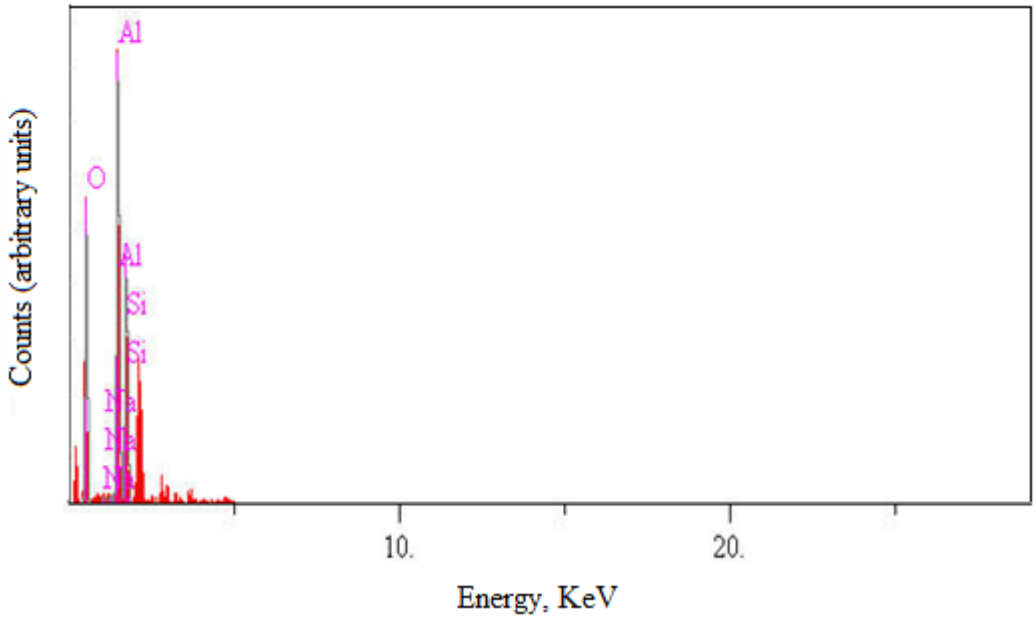

Figure 7.11 EDS analysis diagram of sample without additive after firing

Figure 7.12 shows microstructure of RP- AP sample. Ramanenka (2011) considered that when Al_2O_3 is added into refractory, andalusite (Al_2SiO_5) is turned into mullite

excess silica is released as amorphous silica. Most of amrphous silica is trapped in the mullite grains as “islands” and capillaries. Capillaries were observed in RP-AP structure. Figure 7.13 shows EDS analysis diagram of sample 10 wt. % Al_2O_3 additive after firing.

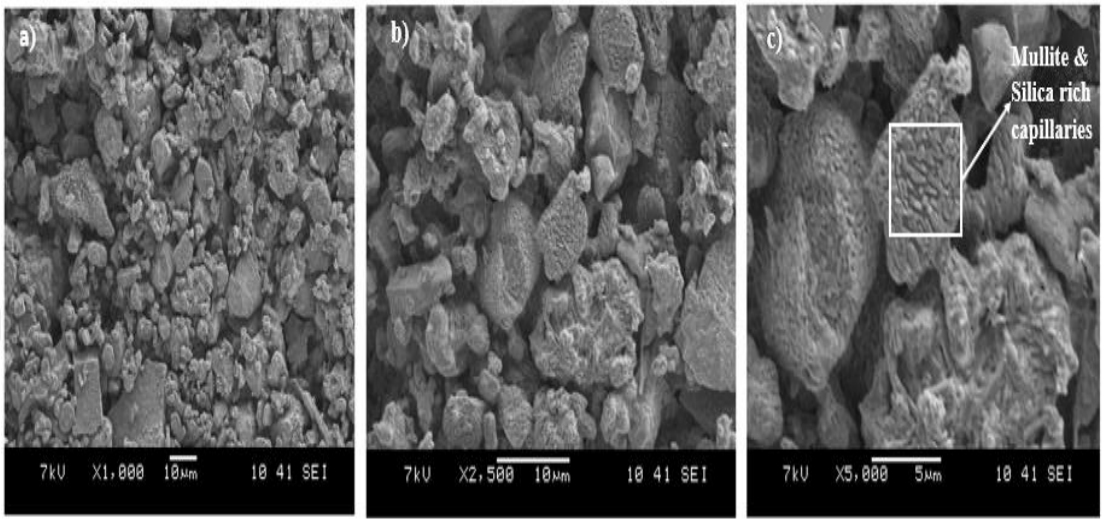

Figure 7.12 Scanning electron microscopy images of the region with 10 wt. % Al_2O_3 additive after firing and analyzed EDS (a) X1000; (b) X2500; (c) X5000 magnification indicates, respectively

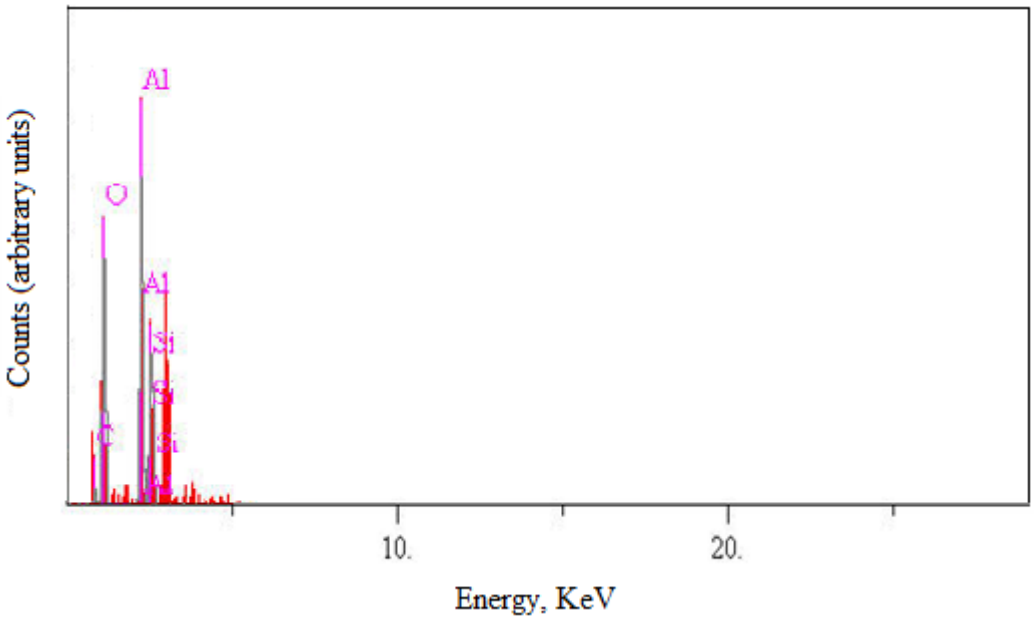

Figure 7.13 EDS analysis diagram of sample 10 wt. % Al_2O_3 additive after firing

Figure 7.14 shows microstructure of RP-TP sample. Dense and compact microstructure was obtained for RP-TP. TiO_2 is uniformly distributed on the surface. Figure 7.15 shows EDS analysis diagram of sample 1 wt. %TiO_2 additive after firing (Bezir et al., 2020).

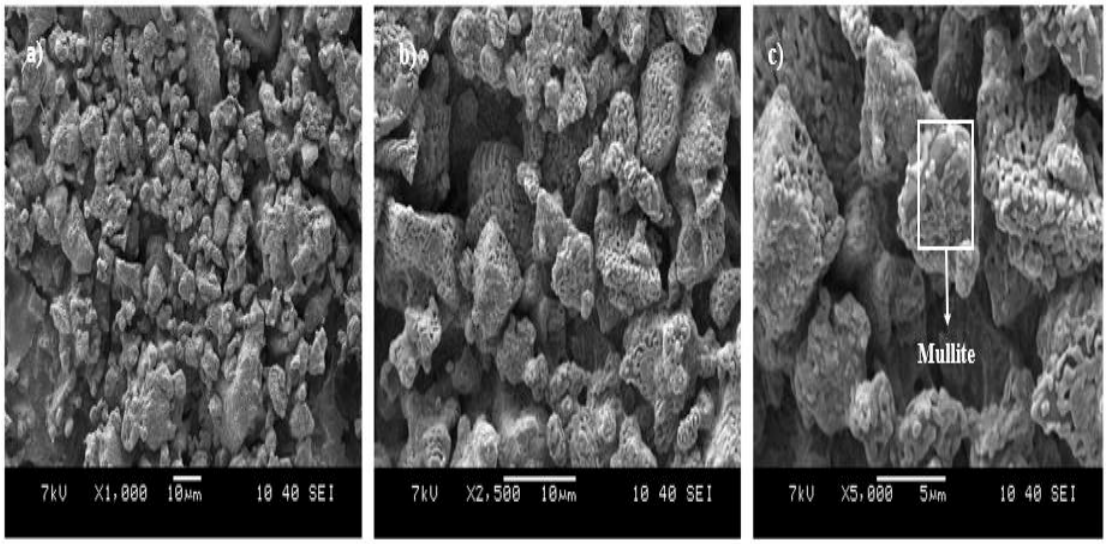

Figure 7.14 Scanning electron microscopy images of the region with 1 wt. %TiO_2 additive after firing and analyzed EDS (a) X1000; (b) X2500; (c) X5000 magnification indicates, respectively

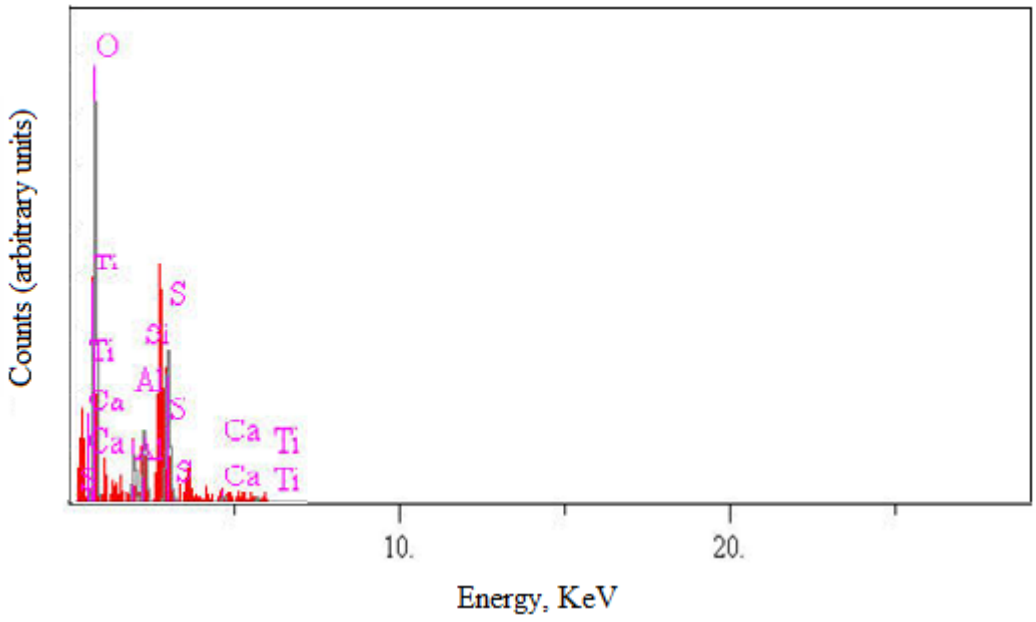

Figure 7.15 EDS analysis diagram of sample 1 wt. %TiO_2 additive after firing

Figure 7.16 shows microstructure of RP-AP-TP sample. Darkest regions is alumina and dark gray is mullite, while white regions are titanium according to EDS analysis shown in figure 7.17.

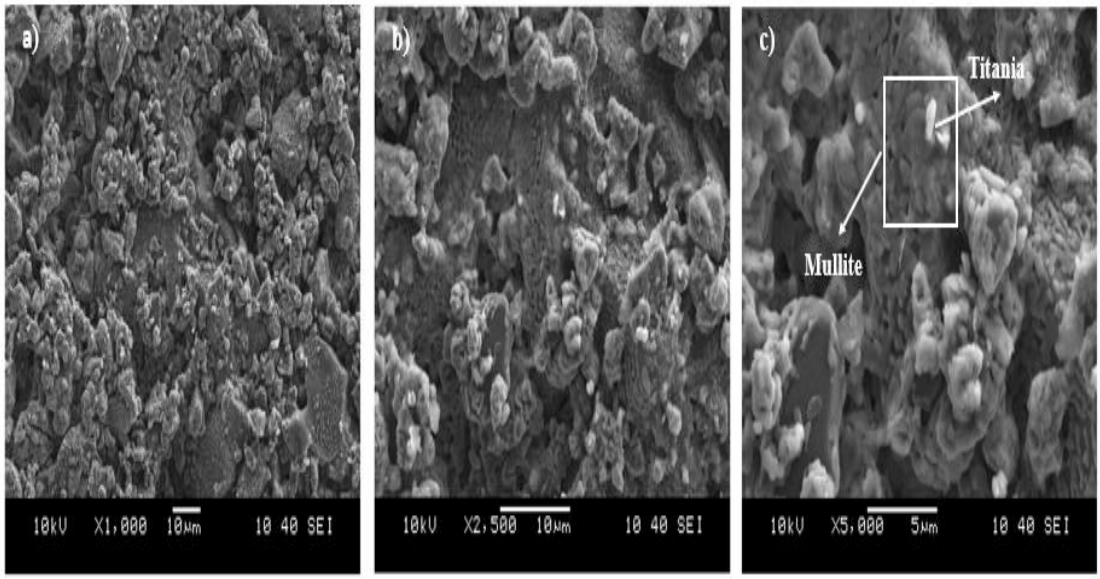

Figure 7.16 Scanning electron microscopy images of the region with 1 wt. % TiO_2 and 10 wt. % Al_2O_3 additive after firing and analyzed EDS (a) X1000; (b) X2500; (c) X5000 magnification indicates, respectively

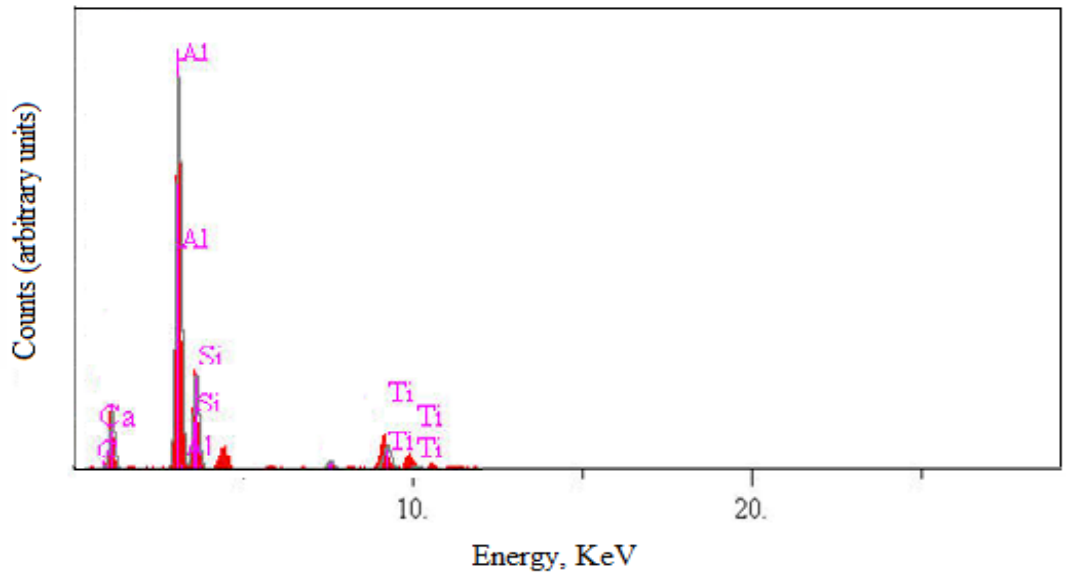

Figure 7.17 EDS analysis diagram of sample with 1 wt. % TiO_2 and 10 wt. % Al_2O_3 additive after firing

It is clear from figure 7.18 that porosity increased with graphite addition. Partial and porous structure was observed in RP- GCP and RP- TP- GCP. Eustathopoulos et al. (1974) thought that oxidation of graphite lead to porosity. Figure 7.19 shows EDS analysis diagram of sample with 10 wt. % graphite additive after firing.

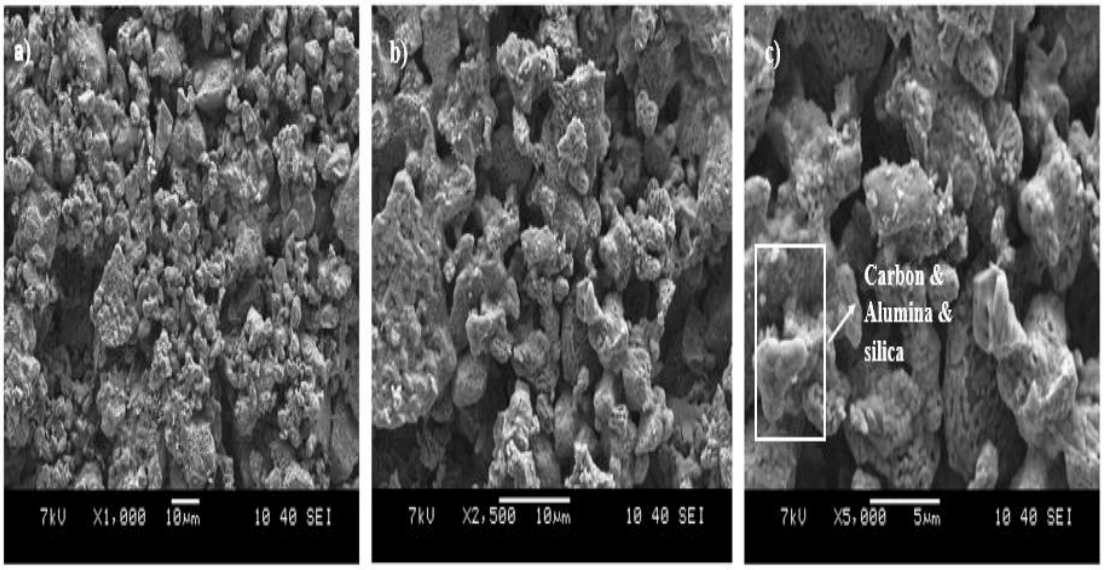

Figure 7.18 Scanning electron microscopy images of the region with 10 wt. % graphite additive after firing and analyzed EDS (a) X1000; (b) X2500; (c) X5000 magnification indicates, respectively

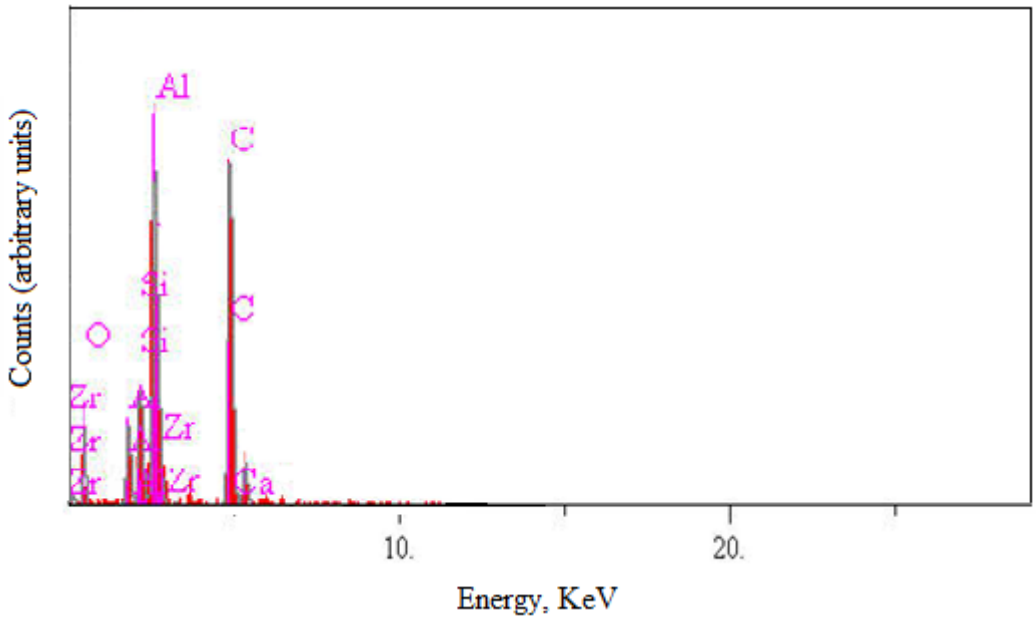

Figure 7.8 EDS analysis diagram of sample with 10 wt. % graphite additive after firing

Figure 7.20 shows microstructure of RP- TP- GCP. Sample's structure is porous in RP-TP- GCP likewise to RP- GCP. Black regions indicate voids in structure. It was observed a discontiguous network with interlocked crystallites (Hoseinpur & Safarian, 2020). However, sporadic pores are still in structure. Figure 7.21 shows EDS analysis diagram of sample with 10 wt. % graphite and 1 wt. %TiO_2 additive after firing.

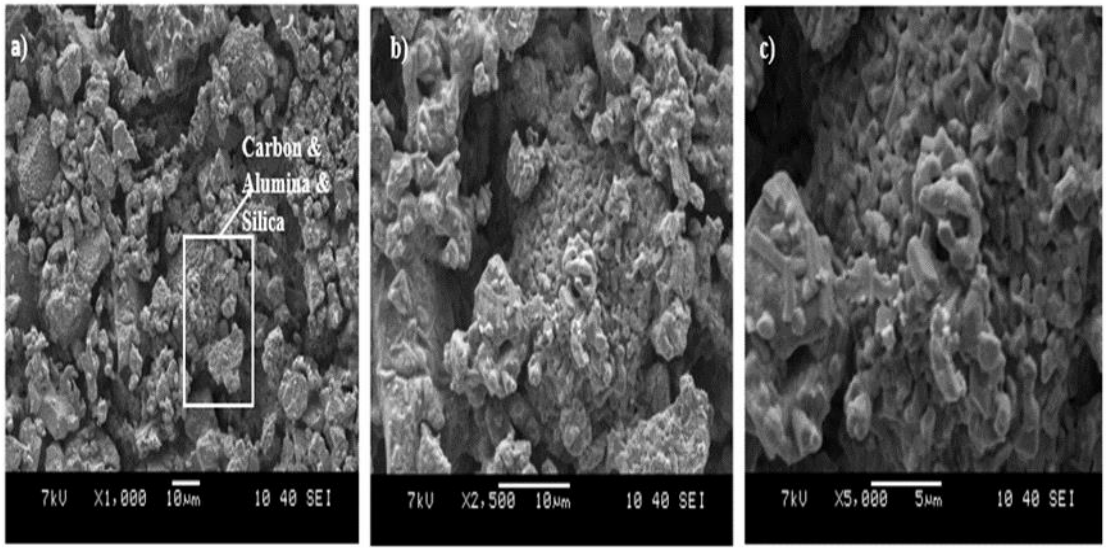

Figure 7.20 Scanning electron microscopy images of the region with 10 wt. % graphite and 1 wt. %TiO_2 additive after firing and analyzed EDS (a) X1000; (b) X2500; (c) X5000 magnification indicates, respectively

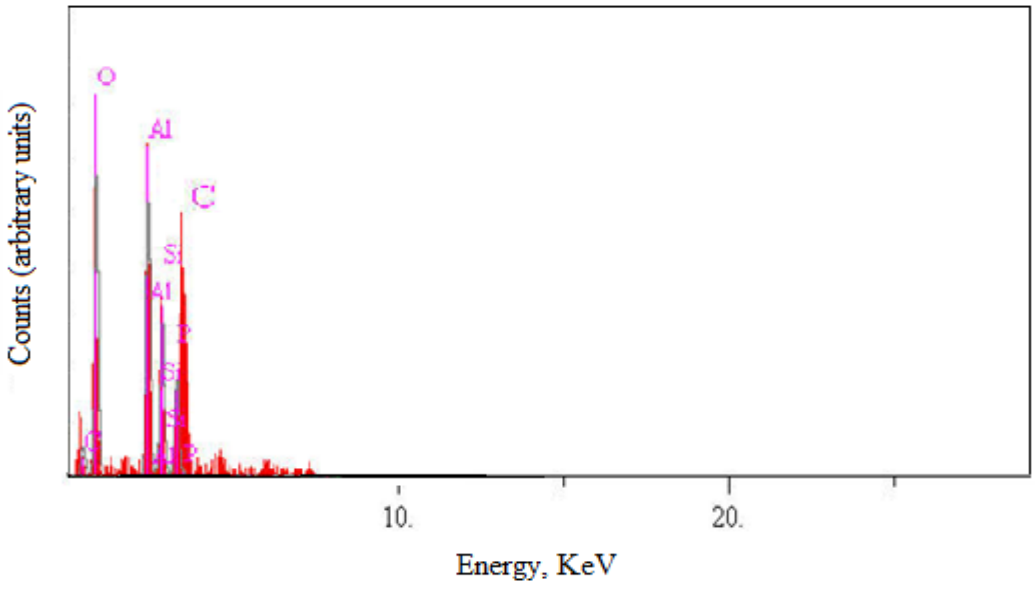

Figure 7.21 EDS analysis diagram of sample with 10 wt. % graphite and 1 wt. %TiO_2 additive after firing

CHAPTER 8
CONCLUSIONS

8.1 Conclusions

The mechanical, thermal and microstructural properties with graphite, titania and alumina additives on high alumina bricks were investigated the main conclusions can be presented as:

- Graphite addition on high alumina refractory mixture resulted in large pores.
- Samples with titania additives exhibited smallest pores in body, leading to densification.
- The addition of TiO_2 can promote the sintering, increase in bulk density and reduce in apparent porosity of high alumina refractory material. Also, tialite was phase obtained.
- Oxidation of graphite led to a porous material with diminished properties.
- MOR of RP-Al_2O_3, RP-TiO_2 and RP-Al_2O_3-TiO_2 refractory improved.
- HMOR of refractories containing additives decreased according to reference sample.
- Samples' thermal shock performance was found adequate -except for graphite additives.
- Samples except for graphite additives have brought to a successful results according to corrosion test results.
- Best results were obtained from RP-TP and RP-AP-TP mixtures.

8.2 Suggestions

The study suggest the following several objectives to be considered:

- The aluminium slag need to be characterized by XRD to understand chemical characteristics.
- SEM/ EDS analysis for the corrosion test samples need to be planned to investigate the corroded and non-correded areas by slag. It might help to understand reactions with aluminium slag and refractory matrix thoroughly.

- It is suggested that cross section images of each samples should be examined by optical microscope.
- Hindering oxidation experiments with graphite added samples need to be planned in order to observe reactions with graphite additive refractory and aluminium melt.

REFERENCES

Allahevrdi, M., Afshar, S., & Allaire, C. (1998). Additives and the corrosion resistance of aluminosilicate refractories in molten Al-5Mg. *The Journal of The Minerals, Metals & Materials Society*, *50*(2), 30–34.

Allaire, C. (2000). Refractories for molten aluminum confinement. *Canadian Ceramics*, *69*(1), 14–21.

Banerjee, S. (1998). *Monolithic refractories: a comprehensive handbook.* Singapore: World Scientific.

Bezir, N. Ç., Akar, V., Özkorucuklu, S. P., Yildirim, G., Evcin, A., & Ceylan, O. (2020). Application of TiO_2 dye-sensitive solar cells by electrochemical storage method. *Acta Physica Polonica A*, *137*(4), 513–518.

Brochen, E., Clasen, S., Dahlem, E., & Dannert, C. (2017). Determination of the thermal shock resistance of refractories. *Asocicación Nacional de Fabricantes de Refractarios*, Retrieved December 25, 2020, from http://www.anfre.com/pdf/determination-of-the-thermal-shock-resistance-of-refractories.pdf

Brondyke, K. J. (1953). Effect of molten aluminum on Alumina-silica refractories. *Journal of the American Ceramic Society*, *36*(5), 171–174.

Car, E. (2008). *Alüminyum üretim süreçlerinde kullanılan ergitme ve tutma fırınlarına genel bir bakış.* Retrieved December 25, 2020, from https://docplayer.biz.tr/5093784-Aluminyum-uretim-sureclerinde-kullanilan-ergitme-ve-tutma-firinlarina-genel-bir-bakis-erman-car.html

Chen, M., Shen, M., Wang, X., Zhu, S., & Wang, F. (2012). Oxidation and thermal shock behavior of a glass-alumina composite coating on K38G superalloy at 1000 °C. *Journal of Materials Science and Technology*, *28*(5), 433–438.

De Villiers, J. P., Mulange, D., & Garbers-Craig, A. M. (2020). The Effect of titanium oxide additions on the phase chemistry and properties of chromite-magnesia Refractories. *Ceramics*, *3*(1), 127–143.

Ewais, E. M. M. (2004). Carbon based refractories. *Journal of the Ceramic Society of Japan*, *112*(1310), 517–532.

Furness, A. G., & Pygall, C. F. (1983). Hot face refractory failure in aluminium melting and holding furnaces. *Transactions and Journal of the British Ceramic Society*, *82*(6), 213-215.

Gaertner, J., & Boeker, R. (2015). Retrieved December 25, 2020, from http://www.alumag.com/wpcontent/uploads/2015/11/3AluMagNASymposium15_Striko_Westofen_America.pdf

Hemrick, J. G., Headrick, W. L., & Peters, K. M. (2008). Development and application of refractory materials for molten aluminum applications. *International Journal of Applied Ceramic Technology*, *5*(3), 265–277.

Johnson, S. M., & Pask, J. A. (1982). Formation of mullite in kaolinite and Al_2O_3-SiO_2 mixtures. *Journal of the American Ceramic Society. 61*(8), 838–842.

Juhasz, K. L., Baumli, P., Sytchev, J., & Kaptay, G. (2013). Wettability of graphite by liquid aluminum under molten potassium halide fluxes. *Journal of Materials Science*, *48*(21), 7679–7685.

Koshy, P. (2009). *Effect of chemical additives on the interfacial phenomena of high alumina refractories with Al-alloys*. PhD Thesis, The University of New South Wales, Australia.

Liu, Z., Deng, C., Yu, C., Wang, X., Ding, J., & Zhu, H. (2019). Molten salt synthesis and characterization of SiC whiskers containing coating on graphite for application in Al_2O_3-SiC-C castables. *Journal of Alloys and Compounds*, *777*, 26–33.

Meyer-Rau, S., & Telle, R. (2005). Testing strategies for corrosive interactions of ceramics with semi-solid and molten metal alloys. *Journal of the European Ceramic Society*, *25*(7), 1049–1055.

Nemati, Z. A., & Moetakef, P. (2007). Investigation of graphite oxidation kinetics in MgO–C composite via artificial neural network approach. *Computational Materials Science*, *39*(4), 723-728.

Oliveira, M., Agathopoulos, S., & Ferreira, J. M. F. (2002). Reactions at the interface between Al_2O_3-SiO_2 ceramics with additives of alkaline-earth oxides and liquid Al-Si alloy. *Journal of Materials Research, 17*(3), 641–647.

Pereira, P. F. A., & Baldo, J. B. (1997). A low cement aluminum silicate refractory castable with improved resistance to molten aluminum and cryolite. *Unified International Technical Conference on Refractories, 97,* 1667-1676.

Routschka, G. (2008). *Refractory materials: pocket manual; design, properties, testing* (3rd ed.). Essen: Vulkan-Verlag GmbH.

Schacht, C. (2004). *Refractories handbook*. USA: CRC Press.

Siljan, O. J., Schoning, C., & Grande, T. (2002). State-of-the-art alumino-silicate refractories for Al electrolysis cells. *The Journal of The Minerals, Metals & Materials Society (TMS), 54*(5), 46-55.

Sobczak, N., Stobierski, L., Radziwill, W., Ksiazek, M., & Warmuzek, M. (2004). Wettability and interfacial reactions in Al/TiO_2. *Surface and Interface Analysis, 36*(8), 1067–1070.

Sun, Y., Li, Y., Zhang, L., Li, S., Yan, M., & Sun, J. (2019). Novelty phase synthesis mechanism and morphology in resin-bonded Al-Al_2O_3-TiO_2 composites at high temperatures under flowing N_2. *International Journal of Minerals, Metallurgy and Materials, 26*(9), 1177–1185.

Volceanov, E., Gurban, A. M., Volceanov, A., & Ni, P. (2004). High thermal shock resistant aluminium titanate type ceramics. *Key Engineering Materials, 268*, 993–996.

Wei, Y., Dong, Y., Zhang, T., Chen, J., & Yan, W. (2020). Influence of reaction of Al_2O_3 and carbonaceous materials in Al_2O_3–C refractories on aluminum and carbon pick-up of iron. *Journal of Iron and Steel Research International*, *27*(1), 55–61.

Yamaguchi, A. (1987). Thermochemical analysis for reaction processes of aluminium and aluminium-compounds in carbon-containing refractories. *Taikabutsu Overseas*, *7*(2), 11.

Yılmaz, Ş., Toplan, H. Ö., & Demirkıran, A. Ş. (2016). *Refrakter malzemeler*. Retrieved December 25, 2020, from https://docplayer.biz.tr/13628900-11-refrakter-malzemeler.html.

Yoshimatsu, H., Fujiwara, S., Konishi, R., Miyawaki, M., & Miura, Y. (1995). Wettability by water and oxidation resistance of alumina-coated graphite powder. *Journal of the Ceramic Society of Japan, 103*(1201), 929-934.

Yuan, W., Tang, H., Shang, H., Li, J., Deng, C., & Zhu, H. (2017). Effects of TiO_2 addition on kinetics of in situ spinel formation and properties of alumina-magnesia refractory castables. *Journal of Ceramic Science and Technology*, *8*(1), 121–128.

Zhang, S., Marriott, N. J., & Lee, W. E. (2001). Thermochemistry and microstructures of MgO-C refractories containing various antioxidants. *Journal of the European Ceramic Society*, *21*(8), 1037–1047.

Zhang, S. (2007). Next generation carbon-containing refractory composites. *Industrial Ceramics*, *27*(1), 15–20.

Zhang, S., Hashimoto, S., & Lee, W. E. (2005). Hydration of aluminum powder in magnesia-containing water. *Journal of the American Ceramic Society*, *88*(4), 1057–1059.